공 학 박 사 학 위 논 문

Properties and Mechanisms of Electrochemical Reactive Oxygen Species Generation Using a Solid Polymer Electrolyte Electrolyzer

고체 고분자 전해질 전해조를 이용한 전기화학적 활성산소종 발생 특성 및 메커니즘

2014년 2월

서울대학교 대학원

화학생물공학부

최 주 솔

Properties and Mechanisms of Electrochemical Reactive Oxygen Species Generation Using a Solid Polymer Electrolyte Electrolyzer

by

Jusol Choi

under the supervision of

Professor Jeyong Yoon, Ph. D.

A dissertation submitted in partial fulfillment of the requirements for the Degree of
Doctor of Philosophy

FEBURARY 2014

SCHOOL OF CHEMICAL AND BIOLOGICAL ENGINEERING
SEOUL NATIONAL UNIVERSITY

Properties and Mechanisms of Electrochemical Reactive Oxygen Species Generation Using a Solid Polymer Electrolyte Electrolyzer

고체 고분자 전해질 전해조를 이용한 전기화학적 활성산소종 발생 특성 및 메커니즘

지도교수 윤 제 용

이 논문을 공학박사 학위논문으로 제출함

2013년 10월

서울대학교 대학원

공과대학 화학생물공학부

최 주 솔

최주솔의 공학박사 학위논문을 인준함

2013년 12월

위 원 장 _____ (인)

부 위 원 장 _____ (인)

위 원 _____ (인)

위 원 _____ (인)

위 원 _____ (인)

ABSTRACT

Electrochemical ozone production (EOP) via oxidation of water has attracted attention as an effective technology for a water treatment alternative to the conventional ozonation. The presence of inert supporting electrolytes (SEs) in EOP is essential to increase the electrical conductivity of water, but little is known about the role of SEs in EOP on BDD electrodes. Also, development of electrodes for hydrogen peroxide production via reduction of oxygen was required for simultaneous production of ozone and hydrogen peroxide. In order to expand the knowledge of the effect of SEs on EOP on a BDD electrode and the development of electrodes for hydrogen peroxide production, the following studies were conducted.

First, an effect of SEs on EOP on a BDD electrode was investigated as the solid polymer electrolyte electrolyzer permitting water oxidation even in the absence of SEs was employed. As major results, SEs caused significant suppression of EOP regardless of their types in comparison with that in deionized water, but did not decrease the production of •OH which is intermediate for ozone production and the overall oxidation current. On the other hand, the production of hydrogen peroxide via the combination of •OH was suppressed by the presence of SE. The suppression of EOP by SE is interpreted to be attributed to SE anions hindering the combination of •O on the electrode surface. Based on this suppression effect

of SEs, operating conditions for optimal EOP were investigated.

Second, high-yield hydrogen peroxide generation using a membrane electrode assembly (MEA) with a carbon fiber (CF)-coated mesh substrate was investigated in a solid polymer electrolyte electrolyzer. Current efficiency (52%) and power consumption (0.3 $Wh \cdot g^{-1}$) for this MEA were 1.5 times higher and 2 times lower than those of reported values (at -0.1 V vs. Ag/AgCl). These significant improvements were presumed to be attributed to enhanced oxygen mass transfer and reduced charge transfer resistance arising from the CF-coated mesh substrate in the MEA. Based on these findings, commercial carbon cloth electrodes were employed for hydrogen peroxide production.

Keywords: Hydroxyl radical, ozone, hydrogen peroxide, boron doped diamond electrode, carbon fiber, solid polymer electrolyte electrolyzer.

Student number: 2009-31267

CONTENTS

List of Figures

List of Tables

1. Introduction

1.1. Research background

Ozone is an environmental friendly and powerful oxidant because it leaves no harmful byproducts after a reaction and exhibits a high redox potential (Arihara et al. 2007, Stucki et al. 1985). Because of this, it has a wide variety of applications in disinfection, cleaning, bleaching, wastewater treatment, and water treatment (Onda et al. 2005, Stucki et al. 1987). The most common technology to produce ozone is the corona discharge process with a relatively low energy consumption (~10 Wh/g of ozone gas)(Arihara et al. 2007). However, this process has several disadvantages such as the production of a low ozone concentration (~2 wt%) and the requirement and management of a cooling system, a drying system, and an ozone diffuser (Cui et al. 2009, Da Silva and Jardim 2006, Da Silva et al. 2003b).

Electrochemical ozone production (EOP) has attracted attention as an alternative to conventional corona discharge ozone production because EOP allows for a high ozone concentration and the direct dissolution of ozone in water, as well as low investment costs (Da Silva et al. 2010, Onda et al. 2005). Electrodes with high oxygen overpotential such as PbO_2 (Amadelli et al. 1999, Da Silva et al. 2006, Da Silva et al. 2010, Tatapudi and Fenton 1993), SnO_2 (Cheng and Chan 2004, Cui et al. 2009, Wang et al. 2005), and boron doped diamond (BDD) electrodes (Arihara et al. 2007, Kraft et al. 2006) have been typically employed as anode materials for EOP.

The presence of inert supporting electrolytes (SEs) in EOP is required to

increase the electrical conductivity of the water. It was reported that the nature of SEs is important to determine the efficiency of EOP; thus, PbO_2 electrodes have been employed (Babak et al. 1994, Da Silva et al. 2003a, Foller and Tobias 1982). The high electronegative anions of SEs such as hexafluorophosphate anions improve the current efficiency of EOP on PbO_2 electrodes (Foller and Tobias 1982). However, little is known about the role of SEs in EOP on BDD electrodes as well as the influence of SE conductivity on EOP for optimal yield despite several studies on EOP using BDD electrodes (Arihara et al. 2006, Arihara et al. 2007, Kraft et al. 2006, Nishiki et al. 2011).

Meanwhile, electrochemical reduction of oxygen to produce hydrogen peroxide should be concerned during EOP in order for efficient use of energy. This is because electrochemical oxidation and reduction reactions are always taken place simultaneously in one electrochemical system. Previously, several studies have been investigated for hydrogen peroxide produced by reduction of oxygen in divided electrochemical systems (Alvarez-Gallegos and Pletcher 1998, Gallegos et al. 2005, González-García et al. 2007, Lobyntseva et al. 2007, Qiang et al. 2002) , in fuel cell systems (Otsuka and Yamanaka 1990, Yamanaka et al. 2002, Yamanaka et al. 2003), and in bioelectrochemical systems (Rozendal et al. 2009). However, studies for electrolyte-free hydrogen peroxide production suffered from rather low current efficiency (~30%) (Murayama and Yamanaka 2011, Yamanaka and Murayama 2008), so that development of effective electrodes is necessary.

1.2. Objectives

The effect of SEs on EOP on a BDD electrode and development of efficient electrodes for hydrogen peroxide production were investigated. To this end, the following extensive studies were carried out.

1. To investigate the effects of various SEs in EOP on the BDD electrode and investigate operating conditions including SE electrical conductivity for optimal yield EOP

For this purpose, the SPE electrolyzer that permits water oxidation even without any supporting electrolytes (SEs) was employed. In order to compare ozone production in solution containing SEs to that in DW, several inert SEs were used such as potassium hydrogen phosphate (KH_2PO_4), potassium nitrate (KNO_3), perchloric acid ($HClO_4$), sodium fluoride (NaF), and hexafluorophosphoric acid (HPF_6). Also, hydroxyl radical scavengers such as t-BuOH and MeOH were used. To characterize EOP on BDD and PbO_2 electrodes, cyclic voltammetry, linear sweep voltammetry, chronocoulometry, and reaction rate constants for hydroxyl radical were measured. Also, in order to investigate operating conditions affecting EOP, EOP was performed as electrodes (BDD and PbO_2), electrical conductivity, flow rate, temperature, and applied current varied. The possible mechanism for suppression of EOP on the BDD electrode by SEs was discussed based on the observations. Also, operating conditions for optimal EOP were suggested.

2. To investigate high yield hydrogen peroxide production in a SPE electrolyzer with a carbon fiber coated mesh substrate and carbon cloth electrodes.

For this purpose, carbon fiber-coated mesh substrates and commercially available carbon fiber were employed as the electrode material in an SPE electrolyzer. Current efficiency and power consumption with a carbon fiber (CF)-coated stainless steel mesh substrate were examined, and compared to the electrode material prepared by the hot press method. Also, various type of carbon cloth electrodes – carbon cloth electrode, perforated carbon cloth electrodes, and stranded carbon cloth electrodes – were examined for current efficiency and power consumption. In order to characterize the electrode materials, linear sweep voltammetry, electrochemical impedance spectroscopy, and chronocoulometry were carried out. Efficient electrode design for hydrogen peroxide generation was discussed based on the observation.

2. Literature review

2.1. Electrochemical reactive oxygen species generation

2.1.1. Mechanisms of hydroxyl radical

Hydroxyl radical, a very powerful oxidant with short lifetime, is produced by electrochemical oxidation of water (Eq. 2-1). Produced hydroxyl radical is partially oxidized to form oxygen (Eq. 2-2), or partially reacts with another hydroxyl radical to form hydrogen peroxide (Eq. 2-3).

$$\bullet OH + H^+ + e = H_2O \qquad \text{at 2.7 V vs. NHE} \qquad \text{Eq. 2-1}$$

$$1/2\ O_2 + H^+ + e = \bullet OH \qquad \text{Eq. 2-2}$$

$$\bullet OH + \bullet OH = H_2O_2 \qquad \text{Eq. 2-3}$$

Hydroxyl radical formation by electrochemical oxidation of water depends on anodes (MO_x) that are divided into active and inactive electrodes; hydroxyl radical that is produce by water oxidation is chemically bonded to the active electrodes, resulting in higher oxide formation (MO_{x+1}) (Comninellis 1994b, Simond et al. 1997). However, hydroxyl radical is physically adsorbed on the inactive electrodes, and this hydroxyl radical participates in oxidation of pollutants. Dimensionally stable anodes (DSAs) such as IrO_2 and RuO_2 are the active electrodes that are effective for electrochemical oxygen or chlorine generation due to low oxygen overpotential. PbO_2, SnO_2, and BDD are inactive

electrodes that show good performance of electrochemical ozone generation.

2.1.2. Mechanisms of ozone

Since EOP from the electrolysis of water was first reported by Schönbein in the early 1800's (Rubin 2001), the EOP mechanism has been intensively studied. For example, $^{\bullet}OH$ formation, the intermediate for ozone, was investigated during EOP on PbO_2 electrodes (Wabner and Grambow 1985), and adsorbed oxygen species on the PbO_2 electrodes were deduced (Foller and Tobias 1982, Kotz and Stucki 1987). Based on these findings, the commonly accepted mechanism for EOP was suggested as follows (Babak et al. 1994).

$$H_2O \rightarrow (^{\bullet}OH)_{ads} + H^+ + e^- \quad \text{Eq. 2-4}$$

$$(^{\bullet}OH)_{ads} \rightarrow (^{\bullet}O)_{ads} + H^+ + e^- \quad \text{Eq. 2-5}$$

$$(^{\bullet}O)_{ads} + (^{\bullet}O)_{ads} \rightarrow O_2 \quad \text{Eq. 2-6}$$

$$(^{\bullet}O)_{ads} + (O_2)_{ads} \rightarrow O_3 \quad \text{Eq. 2-7}$$

In the case of the PbO_2 electrode, it has been suggested that $^{\bullet}OH$ generated via oxidation of water (Eq. 2-4)) is absorbed on the PbO_2 surface, and it facilitates ozone production (Reaction Eq. 2-5 – Eq. 2-7). On the other hand, in the case of the BDD electrode, it was explained that $^{\bullet}OH$ is weakly bound to the surface of the BDD electrode because of its inert property, and as a result, ozone formation on the BDD surface is not favored (Michaud et al. 2003). In addition, $^{\bullet}OH$ on the BDD electrode involves the formation of hydrogen peroxide via the combination of $^{\bullet}OH$ (Eq. 2-8) (Marselli et al. 2003, Michaud et al. 2003).

$$^{\bullet}OH + {}^{\bullet}OH \rightarrow H_2O_2 \qquad \text{Eq. 2-8}$$

2.1.2.1. Investigation of ozone production mechanisms

Step 1 can be examined with the result in the previous publication (Wabner and Grambow 1985), as shown in Fig. 2-1 that shows bleaching of RNO by hydroxyl radicals at the PbO_2 anode in phosphate and phosphate with 10% ethanol. As shown in Fig. 2-1, RNO was not bleached with 10% ethanol, and this leaded to no ozone production even though ozone production data were not shown.

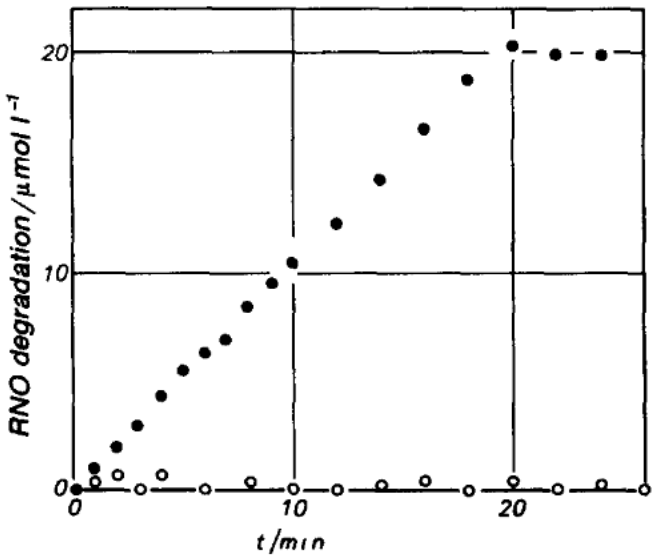

Figure 2-1. RNO beaching by hydroxyl radicals at the PbO_2 anode (current cut off after 20 min). (●)RNO + phosphate buffer; (○) same with 10% ethanol (Wabner and Grambow 1985).

2.1.2.2. Investigation of adsorbed oxygen species

Intermediate oxygen species (Step 2) was speculated and examined with the results in the previous publications ((Babak et al. 1994, Foller and Tobias 1982, Foller and Tobias 1981, Kotz and Stucki 1987). Figure 2-2 (Foller and Tobias 1981) shows the relationship between phosphorous-containing coverage of the PbO_2 anode surface and ozone current efficiency in 2 M H_3PO_4 (A: phosphorous-containing coverage as a function of current density, B: seven discrete polarizations, C: one experiment, polarizing in ascending steps of current density). As shown in Fig. 2-2, high current efficiency of electrochemical ozone production was achieved with low surface coverage of phosphate, while the low current efficiency was achieved with the high surface coverage. It was explained that oxygen intermediate competes with phosphate on available adsorption sites.

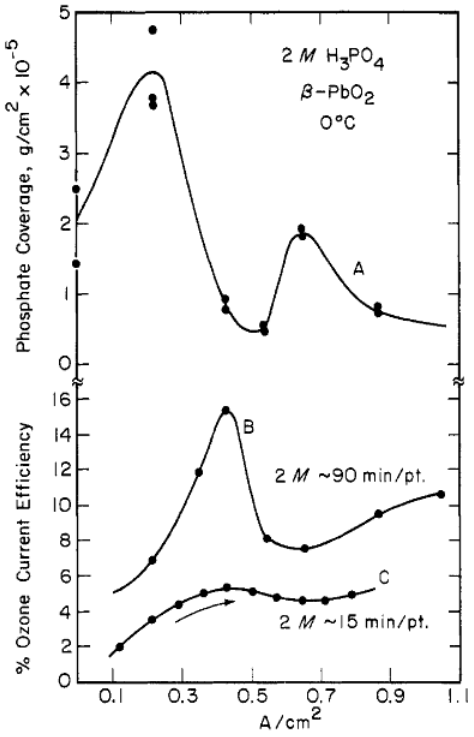

Figure 2-2. The relationship between phosphorous-containing coverage of the PbO_2 anode surface and ozone current efficiency in 2 M H_3PO_4 (A: phosphorous-containing coverage as a function of current density, B: seven discrete polarizations, C: one experiment, polarizing in ascending steps of current density) (Foller and Tobias 1981)

Figure 2-3 (Foller and Tobias 1982) shows the relationship between current efficiency of electrochemical ozone generation and anion electronegativity. As shown in Fig. 2-3, current efficiency of electrochemical ozone production was linearly increased with increasing electronegativity of anions. This is because as anions with high electronegativity would not easily adsorbed on the electrode surface, so that more oxygen intermediate would adsorbed on the surface, resulting in high ozone production.

Figure 2-4 (Babak et al. 1994) shows Tafel plots for the PbO_2 electrode in (a) 0.1 M $NaNO_3$ and (b) 0.1 M $NaNO_3$ + 4 × 10^{-3} M $NaClO_4$. As shown in Fig 2-4, two slopes were obtained at low current range and high current range, indicating that two electrochemical reactions occur (step 1 and 2). The slopes for 0.1 M $NaNO_3$ and 0.1 M $NaNO_3$ + 4 × 10^{-3} M $NaClO_4$ at low current range were not changed, corresponding to step 1. In contrast, the slopes for 0.1 M $NaNO_3$ + 4 × 10^{-3} M $NaClO_4$ at high current range was changed as compared to that for 0.1 M $NaNO_3$. This indicates that electrochemical ozone production occurs in two electrochemical reactions, and the second reaction is affected by anions.

Oxygen intermediate species was measured by capacitance, and Figure 2-5 shows capacity versus potential curves for the PbO_2 electrode ((a) the capacity is measured in 0.1 M $NaNO_3$, from 1.6 V in the distance of less positive potential (b) electrode scanned from 1.6 to 2.1 V at 0.5 mV/s stopped at 1.6 V for 1 min and capacity measured as in (a), (c) same as (b) but 1.4 × 10^{-3} M Na_2SO_4 added as the

potential was held at 1.6 V before recording the capacity. (d) same as (c) with 2.5 × 10^{-3} M Na_2SO_4, (e) experiment carried out as in (b) but with 1.5 × 10^{-3} M Na_2SO_4 added from the beginning) (Babak et al. 1994). As shown in Fig. 5, capacity, after oxygen or ozone generation, was increased as compared to other cases, indicating that ozone or oxygen generation was proceeded with oxygen intermediate adsorption on the electrode surface.

Step 3 and 4 was not examined with the experimental results, but they were assumed with ozone generation mechanisms in gas phase. Ozone was generated by the reaction of oxygen with atomic oxygen in gas phase. Thus, the similar reactions to step 3 and 4 might be speculated (Kotz and Stucki 1987).

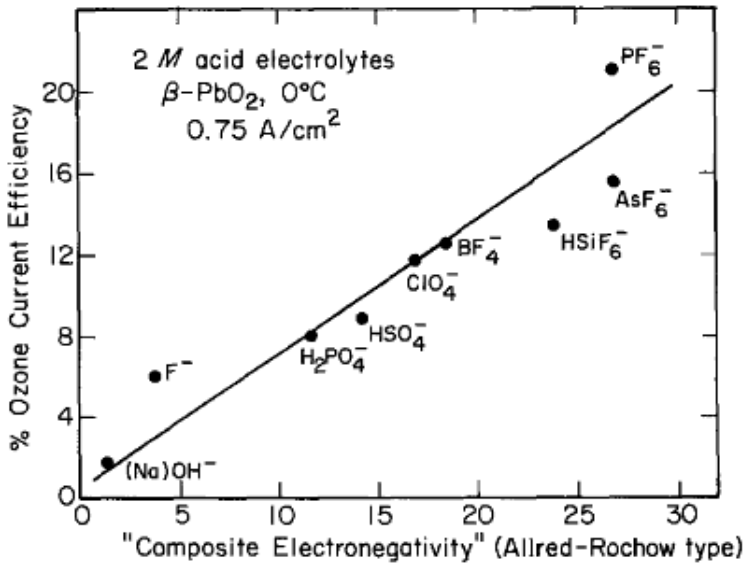

Figure 2-3. The correlation of anion electronegativity and ozone yield using PbO_2 anodes (current efficiency taken during polarization at a single current density of 0.75 A/cm^2 per experiment) (Foller and Tobias 1982)

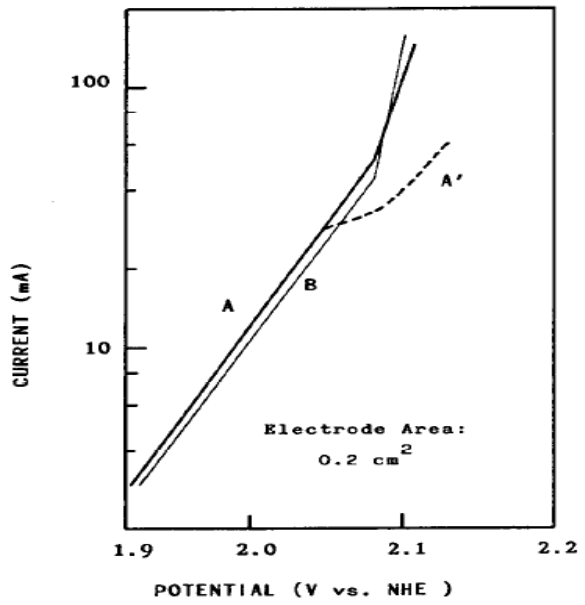

Figure 2-4. Tafel plot for PbO_2 at room temperature and neutral pH (electrode area: 0.2 cm^2, (a) 0.1 M $NaNO_3$, (b) 0.1 M $NaNO_3$ + 4 × 10^{-3} M $NaClO_4$) (Babak et al. 1994)

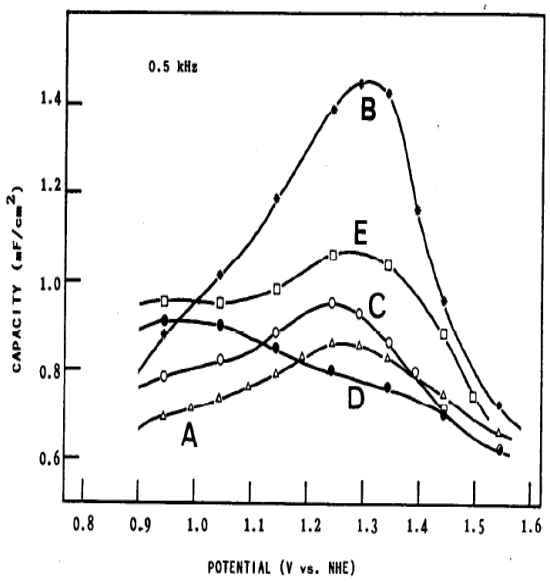

Figure 2-5. Capacity versus potential curves for the PbO_2 electrode ((a) the capacity is measured in 0.1 M $NaNO_3$, from 1.6 V in the distance of less positive potential (b) electrode scanned from 1.6 to 2.1 V at 0.5 mV/s stopped at 1.6 V for 1 min and capacity measured as in (a), (c) same as (b) but 1.4×10^{-3} M Na_2SO_4 added as the potential was held at 1.6 V before recording the capacity. (d) same as (c) with 2.5×10^{-3} M Na_2SO_4, (e) experiment carried out as in (b) but with 1.5×10^{-3} M Na_2SO_4 added from the beginning) (Babak et al. 1994)

2.1.3. Hydrogen peroxide

Hydrogen peroxide is generated by oxidation of water as well as reduction of oxygen. These electrochemical reactions are as follows.

$H_2O_2 + 2H^+ + 2e = 2H_2O$ at 1.78 V vs. NHE Eq. 2-8

$O_2 + 2H^+ + 2e = H_2O_2$ at 0.68 V vs. NHE Eq. 2-9

Since hydrogen peroxide is oxidized to form oxygen at >0.68 V vs. NHE, hydrogen peroxide generation through reduction of oxygen is more practical and the divided reactor is required to achieve high current efficiency (Foller and Bombard 1995). Carbon would be employed for electrode materials for hydrogen peroxide generation due to economic and environmental issues even though gold or mercury could be used (Alvarez-Gallegos and Pletcher 1998, Sánchez-Sánchez and Bard 2009).

2.2. SPE electrolyzer

2.2.1. Properties of SPE electrolyzers

Solid polymer electrolyte (SPE) electrolyzers employing proton exchange membranes were first developed for the purpose of applying space shuttles by general electric company in 1960. (Grigoriev et al. 2006, Grubb 1959, Grubb and Niedrach 1960, Millet et al. 2011, Rasten et al. 2003, Takenaka et al. 1982, Ursúa et al. 2012, Zhang et al. 2007). SPE electrolyzers are considered as the promising technology for generating hydrogen (Cruz et al. 2011, Wei et al. 2010). These electrolyzers have many applications such as fuel cells, hydrogen welding, manufacture of pure substances (Grigoriev et al. 2006). Moreover, another application is to generate oxidants by water splitting in the electrolyzer.

SPE electrolyzers have several advantages for electrochemical oxidant generation. First of all, the SPE electrolyzers permit deionized water (DW) oxidation without any supporting electrolytes (SEs), making possible uses of ozone in cleaning agent for semi-conductor industries. Moreover, products generated on the anode and cathode surface are separated by the SPE. In addition, they show process versatility, energy effectiveness, and environmental compatibility (Rajeshwar et al. 1994). These advantages make the SPE electrolyzers competitive and feasible to other methods to generate oxidants

2.2.2. Membrane electrode assembly (MEA)s

Figure 2-6 shows the cross sectional view of an MEA with electrochemical reactions in an SPE electrolyzer. As shown in Fig. 2-6, the MEA consists of a cathode, a Nafion, and an anode that were sandwiched. In this MEA, electrochemical reactions occur on the thee-phase boundary, the intersection of an electrode, a Nafion, and reactants (Arihara et al. 2007, Takenaka et al. 1982, Yamanaka and Murayama 2008, Zhang et al. 2007). In the case of water splitting, water is oxidized to from oxygen, protons, and electrons in the anode, and then protons penetrated through the Nafion are reduced with electrons in the cathode. The MEA plays a key role in an SPE electrolyzer, so that preparing MEAs that are prepared by chemical plating method, hot press method, and coating catalysts on to backing/current collector is significant (Arihara et al. 2007, Takenaka et al. 1982, Yamanaka and Murayama 2008, Zhang et al. 2007).

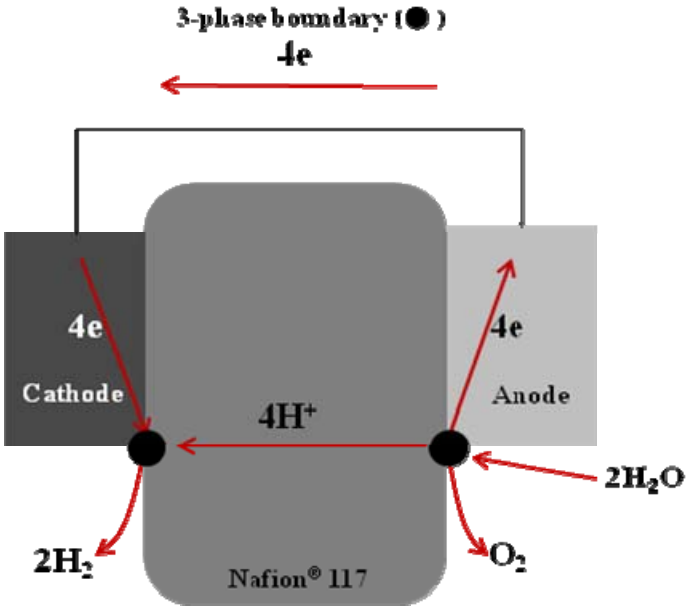

Figure 2-6. The cross sectional view of a membrane electrode assembly (MEA) with electrochemical reaction of water splitting

Figure 2-7 shows the structure of perfluorosulfonate polymer (Nafion®). As shown in Fig. 2-7, sulfonic groups are responsible for proton conduction in the Nafion (Goñi-Urtiaga et al. 2012, Ursúa et al. 2012), and the conductivity of the Nafion 117 in water at room temperature was reported at around 0.1 S/cm (Slade et al. 2002). Because of this, water splitting without addition of any supporting electrolytes occurs in SPE electrolyzers, one of unique characteristics (Grimm et al. 2000, Ursúa et al. 2012, Wei et al. 2010). In addition to this, other characteristics are energy efficiency, compact design, specific production ability, and low operating temperature in comparison with alkaline electrolyzers (Cruz et al. 2011, Rasten et al. 2003, Siracusano et al. 2011, Takenaka et al. 1982, Tanaka et al. 2005, Wei et al. 2010, Wu et al. 2011, Zhang et al. 2007).

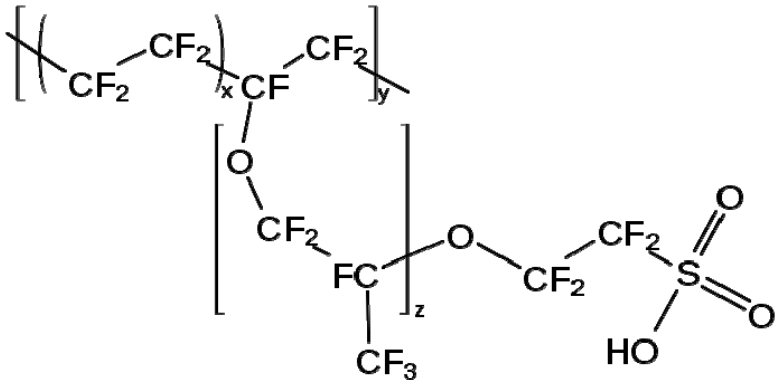

Figure 2-7. Structure of Nafion (http://en.wikipedia.org/wiki/Nafion)

2.2.3. Ozone and hydrogen peroxide generation in an SPE electrolyzer

Ozone–Ozone, a powerful oxidant and no residues after reactions, is an environmental friendly oxidant (Arihara et al. 2007, Onda et al. 2005, Stucki et al. 1985). Owing to this, ozone is employed in many fields such as cleaning of vegetables in hospitals, food industries, or kitchens, disinfection and decolorization of water for industries, water or wastewater treatment, and decomposition of pollutants (Arihara et al. 2007, Onda et al. 2005, Stucki et al. 1987). One of methods to produce ozone is to employ SPE electrolyzers requiring only water without any supporting electrolytes. Advantages of SPE electrolyzers are on-site ozone generation, direct uses of ozone water, and pure ozone water generation (Arihara et al. 2007, Kraft et al. 2006, Stucki et al. 1985, Tatapudi and Fenton 1993). In an SPE electrolyzer, electrochemical reactions for ozone are as follows.

Anodic reaction

$3H_2O \rightarrow O_3 + 6H^+ + 6e^-$ at 1.51 V vs. NHE Eq. 2-10

Cathodic reaction

$4e^- + 4H^+ \rightarrow 2H_2$ at 0.00 V vs. NHE Eq. 2-11

Competitive reaction

$2H_2O \rightarrow O2 + 4\ H^+ + 4e^-$ at 1.23 V vs. NHE Eq. 2-12

Ozone is generated by oxidizing water with protons and electrons in an anode (Eq. 2-10), and hydrogen is formed with protons and electrons in a cathode (Eq. 2-11). Since oxygen evolution is the competitive reaction (Eq. 2-12), high oxygen over potential anodes such as PbO_2, SnO_2, and BDD are required (Foller and Tobias 1982, Michaud et al. 2003).

Current efficiency and power consumption Table 2-1 summarizes current efficiency, power consumption, and electrolysis conditions for ozone generation in SPE electrolyzers from the literature. As shown in Table 2-1, BDD electrodes were employed in few cases though PbO_2 electrodes were commonly used. In the case of BDD, current efficiency was 24 – 47% with cell Potential of ~20 V (Arihara et al. 2007, Kraft et al. 2006). On the other hand, the current efficiency for PbO_2 electrodes was rather low, varying from 5 to 21% with low cell potential of 3 – 5 V (Amadelli et al. 1999, Babak et al. 1994, Da Silva et al. 2006, Da Silva et al. 2010, Onda et al. 2005, Stucki et al. 1987, Stucki et al. 1985, Tatapudi and Fenton 1993).

Table 2-1. Current efficiency, power consumption and conditions of ozone generation in SPE electrolyzers

Reference	Anode	Electrode area (cm^2)	Detecting ozone phase	Electrolyte (anode)	C.E.[a] (%)	P.C.[b] (Wh/g)	C.D.[c] (A/cm^2)	C.P.[d] (V)	F.R.[e] (L/h)	Temp. (^oC)
Stucki et al., 1985	PbO_2(α, β mixture) coated porous Ti	30	Gas, liquid	D.W.	15	~80	1.3	~3.5	10	25
Stucki et al., 1987	PbO_2(α, β mixture) coated porous Ti	30	Liquid	D.W.	20	65	1.3	~3.5	30	30
Tatapudi and Fenton, 1993	β-PbO_2 (7.2mg/cm^2) + Teflon + Platinum (hot press)	13	Gas, liquid	D.W.	~5	50	~1.4	4	28	RT
Babak et al., 1994	β-PbO_2 + 1 % liquid Nafion-spreded on porous Ti	0.2	-	D.W. + NaF 0.08 M	~8	-	1	~4.6	-	RT
Amadelli et al., 1999	F-PbO_2 coated on platinised porous Ti disk	1.5	-	D.W.	~8	-	-	~4.3	-	RT
Onda et al., 2005	multi Ti Plated with PbO_2	10	Gas, liquid	D.W.	12	95	1	~4	33	25
Da Silva et al., 2006	Ti Pt β-PbO_2	80	Gas	3 M H_2SO_4 + 0.03 M KPF_6	21	60	~0.5	~4	1.3 cm/s	0
Kraft et al., 2006	BDD mesh	13	Liquid	D.W.	24	133	0.153	8-23	95	20
Arihara et al., 2007	perofrated BDD (410 holes)	7.5	Liquid	D.W.	47	130~140	1.88-2.5	18-20	120	12
Da Silva et al., 2010	PbO_2 coated stainless steel mesh	90	Gas	D.W.	13	70	1.4	~5.25	1.35cm/s	30

a: current efficiency, b: power consumption, c: current density, d: cell potential, e: flow rate

Figure 2-8 shows power consumption vs. current efficiency of electrochemical ozone production on BDD and PbO_2 electrodes in literature. As shown in Fig. 2-8, BDD appeared to be rather high power consumption with high current efficiency in comparison with PbO_2 showing low power consumptions with low current efficiency. For example, the power consumption of BDD was around 140 Wh/g though the power consumption of PbO_2 varied from 50 to 95 Wh/g with low current efficiency. Power consumption depending on electrode materials can be explained by oxygen overpotential of electrode materials. BDD electrodes showed high oxygen overpotential of 1 V more than PbO_2 electrodes (Da Silva et al. 2003b, Kapałka et al. 2008), resulting high cell potential (~20 V) and power consumption for BDD electrodes.

Silent discharge appears fairly low power consumption (~10 Wh/g, (Arihara et al. 2007)), compared with SPE electrolyzers showing about 1 order of magnitude high power consumption. Thus, power consumption for SPE electrolyzers should be improved to be competitive with silent discharge though the advantage of the SPE electrolyzers such as directly producing ozone water will be found. Two possible directions for the improvement of SPE electrozers can be considered; one is to enhance current efficiency more than currently reported values, so that a trade-off between high current efficiency and high power consumption for SPE electrolyzers might be found due to the cost of dissolving ozone into water for the silent discharge system. This case will correspond to BDD electrodes. Another is

to achieve comparable power consumption of SPE electrolyzers to the silent discharge. This will correspond to PbO_2 electrodes.

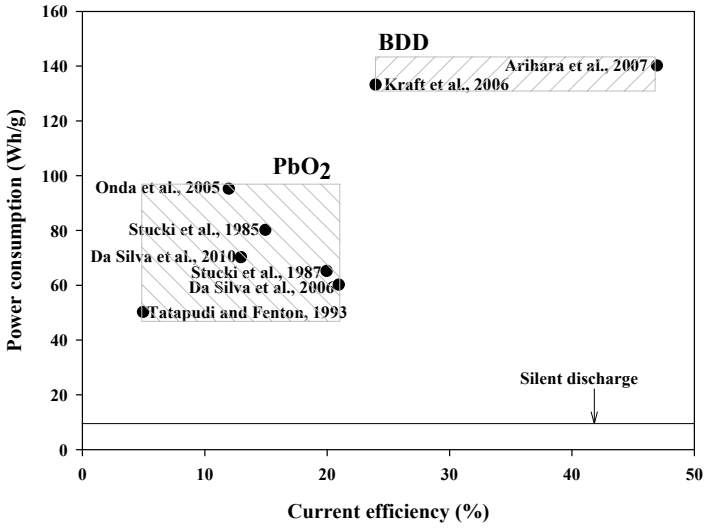

Figure 2-8. Power consumption vs. current efficiency of electrochemical ozone production on BDD and PbO_2 electrodes

Electrolysis conditions for ozone generation in SPE electrolyzers In electrolysis conditions for ozone generation in SPE electrolyzers, membrane electrode assemblies (MEAs) were prepared with free standing electrodes in many cases though electrode materials were hot pressed on Nafion in few cases. Flow-through reactors were employed with ~1 A/cm^2 at the temperature from 0 to 30 ^oC. Pure water was used as the precursor for ozone generation, and supporting electrolytes such as H_2SO_4, NaF or KPF_6 were used in few cases. Conditions employed for ozone generation such as flow, temperature, and acidity was responsible for ozone dissolution. Ozone decomposition with hydroxyl radical on electrode surface can be prevented with water flow, and ozone solubility is increased with acidic conditions at low temperature as well (Foller and Tobias 1982, Kraft et al. 2006). It is known that NaF and HPF_6 help ozone generation (Foller and Tobias 1982).

Hydrogen peroxide–Hydrogen peroxide is an environmental friendly reagent that produces water after reaction (Alvarez-Gallegos and Pletcher 1998, Lobyntseva et al. 2007, Murayama and Yamanaka 2011, Yamanaka and Murayama 2008). It is used as oxidants or bleaching agents of pulp or paper, in wastewater treatment (Murayama and Yamanaka 2011, Yamanaka and Murayama 2008, Yamanaka et al. 2003). Hydrogen peroxide is conventionally produced by an anthranquinone process, but the effort on producing hydrogen peroxide through electrochemical processes has been made to overcome drawbacks of the conventional process such as cost or safety problems. One candidate to produce hydrogen peroxide is to employ an SPE electrolyzer. Electrochemical reactions for hydrogen peroxide generation in an SPE electrolyzer are as follows.

Anodic reaction

$2H_2O \rightarrow O_2 + 4H^+ + 4e^-$ at 1.23 V vs. NHE Eq. 2-13

Cathodic reaction

$O_2 + 2H+ + 2e^- \rightarrow H_2O_2$ at 0.68 V vs. NHE Eq. 2-14

Competitive reaction

$2H^+ + 2e^- \rightarrow H_2$ at 0.00 V vs. NHE Eq. 2-15

Water is oxidized to form oxygen, protons, and electrons in an anode (Eq. (2-13)), and oxygen is reduced with protons and electrons from an anode to form

hydrogen peroxide (Eq. (2-14)). Hydrogen formation is competitive to hydrogen peroxide formation (Eq. (2-15)), so that electrode overpotential for hydrogen should be high. For this reason, carbon suits the electrode materials though mercury or gold can be used as the electrode materials as well (Foller and Bombard 1995, Gallegos et al. 2005, Meinero and Zerbinati 2006, Sánchez-Sánchez and Bard 2009). Hydrogen peroxide generated in an SPE electrolyzer can be electrolyte-free in the case of pure water oxidation, and then this electrolyte-free hydrogen peroxide is applied to high value-added products such as cleaning semi-conductors or medical instruments.

Current efficiency for H_2O_2 generation- Table 2-2 summarizes current efficiency and electrolysis conditions in SPE electrolyzers or fuel cells from the literature. As shown in Table 2-2, SPE electrolyzers generated hydrogen peroxide with fairly low current efficiency (27 – 31%) in electrolyte-free conditions (Murayama and Yamanaka 2011, Yamanaka and Murayama 2008), but fuel cells showed high current efficiency up to 93% in 2 M NaOH (Yamanaka et al. 2003). In electrolyte free conditions, enhancing functional groups on the carbon materials through acid treatment or coating nafion solution on electrodes was proposed to improve current efficiency of hydrogen peroxide generation (Murayama and Yamanaka 2011, Yamanaka and Murayama 2008). However, the current efficiency for electrolyte-free hydrogen peroxide generation is still comparably low. In this field,

more efforts to improve the current efficiency will be necessary.

Table 2-2. current efficiency and conditions of hydrogen peroxide generation in SPE electrolyzers and fuel cells

Reference	Electrolyte (cathode)	Current efficiency (%)	Applied Potential (V)	Reactor types
Otsuka and Yamanaka, 1990	0.1 N HCl (pH 1.1)	~60	-	Fuel cell(H_2,O_2)
Alvarez-Gallegos and Pletcher, 1998	10 mM H_2SO_4 (pH 2) + 500 mM Na_2SO_4	69	-0.5	SPE electrolyzer
Yamanaka et al., 2003	2 M NaOH	93	-	Fuel cell(H_2,O_2)
Yamanaka et al., 2008a	No catholyte	42	-	Fuel cell(H_2,O_2)
Yamanaka and Murayama, 2008	D.W., No catholyte (VGCF)	26.5	-0.3	SPE electrolyzer
Murayama et al., 2011	No catholyte	42	-	Fuel cell(H_2,O_2)
Murayama and Yamanaka, 2011	D.W. (VGCF)	31	-0.3	SPE electrolyzer

2.2.4. Simultaneous ozone and hydrogen peroxide generation

Electrochemical reduction and oxidation take place simultaneously, so that ozone and hydrogen peroxide will be produced in one electrochemical system, and this will reduce waste of energy. Figure 2-9 shows simultaneous ozone and hydrogen peroxide generation. As shown in Fig. 2-9, hydrogen peroxide is generated by oxygen reduction with protons and electrons at 0.68 V vs. NHE, and ozone is formed by water oxidation at 1.51 V vs. NHE. The net reaction for simultaneous ozone and hydrogen peroxide generation is described as follows.

Net reaction of simultaneous O_3/H_2O_2 generation

: $3H_2O + 3O_2 = O_3 + 3H_2O_2$ Eq. 2-16

Water with oxygen produces ozone by oxidation reaction and hydrogen peroxide by reduction reaction in one electrochemical system at the same time (Eq. 2-16). SPE electrolyzers will make this possible with proper cathode and anode materials, and one report was found in the literature (Tatapudi and Fenton 1994). A PbO_2 as an anode and a gold mesh as a cathode were employed in the SPE electrolyzer, and current efficiencies for ozone and hydrogen peroxide were reported at ~4% and ~0.5% with cell potential of 4.5 V, respectively.

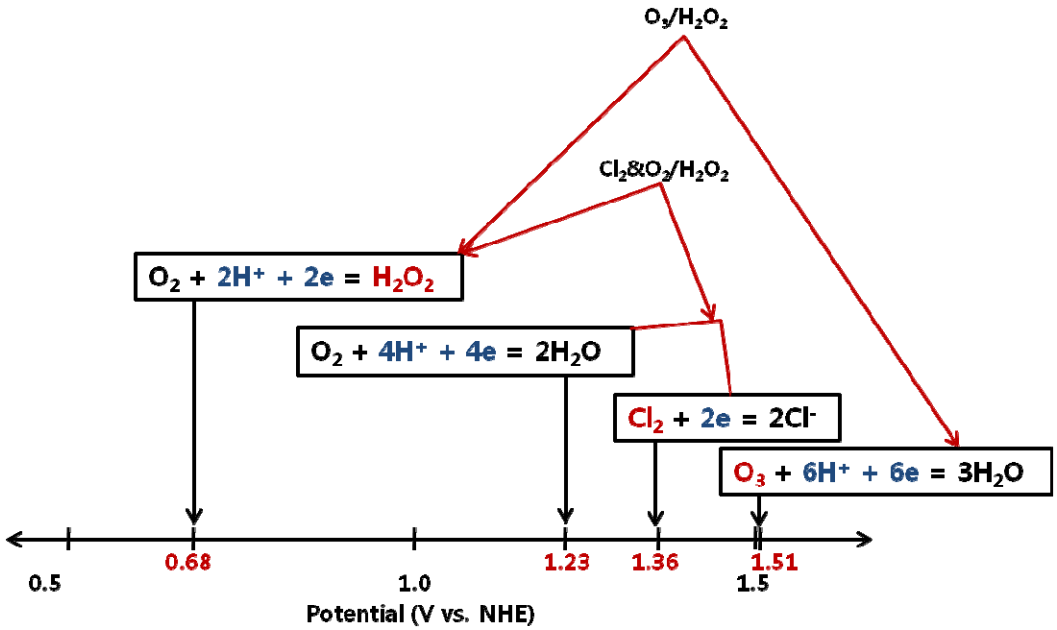

Figure 2-9. Standard redox potentials for oxidants

3. Experimental section

3.1. Chemicals

All chemicals were reagent grade and used without further purification. Deionized water (DW) was used in all experiments (<18 MΩ cm, Milli-Q® Direct 8 system, Millipore, Bedford, MA, USA). N,N-dimethyl-p-nitrosoaniline (RNO) as a probe for hydroxyl radical, tertiary butanol (t-BuOH) and methanol (MeOH) as scavengers for hydroxyl radical, lead nitrate ($Pb(NO_3)_2$), oxalic acid, and nitric acid (HNO_3) were purchased from Sigma-Aldrich Co(St. Louis, MO, USA). Several SEs, potassium hydrogen phosphate (KH_2PO_4), potassium nitrate (KNO_3), perchloric acid ($HClO_4$), sodium fluoride (NaF), and hexafluorophosphoric acid (HPF_6), were employed based on the previous publications (Babak et al. 1994, Foller and Tobias 1982). poly(acrylonitrile) (Mw ~150,000), N,N-dimethylformamide, N-methyl-2-pyrrolidone (NMP), and polyvinylidene fluoride (PVDF) were purchased from Sigma-Aldrich Co. (St. Louis, MO, USA).

3.1.1. Supporting electrolytes

For the selected SEs (KH_2PO_4, KNO_3, $HClO_4$, NaF, and HPF_6), no direct electrochemical oxidation and chemical reactions with hydroxyl radical are found (Bard et al. 1985, Buxton et al. 1988) except KH_2PO_4 with the relatively slow reaction between hydroxyl radical and $H_2PO_4^-$ ($k = 2 \times 10^4$ L/mol·s) (Brillas 2011, Masten et al. 1996, Wu and Masten 2002). However, these SE anions render the current efficiency various from 6 to 22% in EOP on PbO_2 electrodes (Babak et al. 1994). The concentration range of SEs used in this study was in 0.01 mM – 100 mM that was similar or several order of magnitudes lower than previous studies (Da Silva et al. 2003a, Foller and Tobias 1982).

3.2. Electrodes

3.2.1. Preparation of a BDD electrode

The anode for EOP was a commercial boron doped diamond mesh electrode (BDD, apparent area: 8.9 cm^2, wire diameter: 0.1 cm, Condias GmbH, Germany). Figure 3-1 shows Raman spectrum for BDD. As shown in Fig. 3-1, sharp 1332 /cm peak indicates films constituted mainly by diamond crystal.

Figure S1 and S2 show the scheme and the blue print of the SPE electrolyzer used for electrochemical ozone and hydrogen peroxide production in Appendix. Note that the electrolyzer was fabricated in the consideration of the previous publication (Yamanaka and Murayama 2008). As shown in Fig. S1, an anode (BDD mesh), Nafion 117, a cathode (stainless steel mesh) contacted each other between two compartments. For the experiment of EOP, a titanium current collector was used for the anode and the stainless steel mesh was used for the cathode. For the experiment of hydrogen peroxide production, the cathode was switched to the carbon fiber coated-stainless steel mesh electrode. In order to analyze electrochemical reactions, an Ag/AgCl reference electrode was employed. As shown in Fig. S2, a 1 mm-gap exists for the electrode position in the SPE electrolyzer. Two electrodes were pressed each other in this position with the ~1kg/cm^2 of pressure between two compartments..

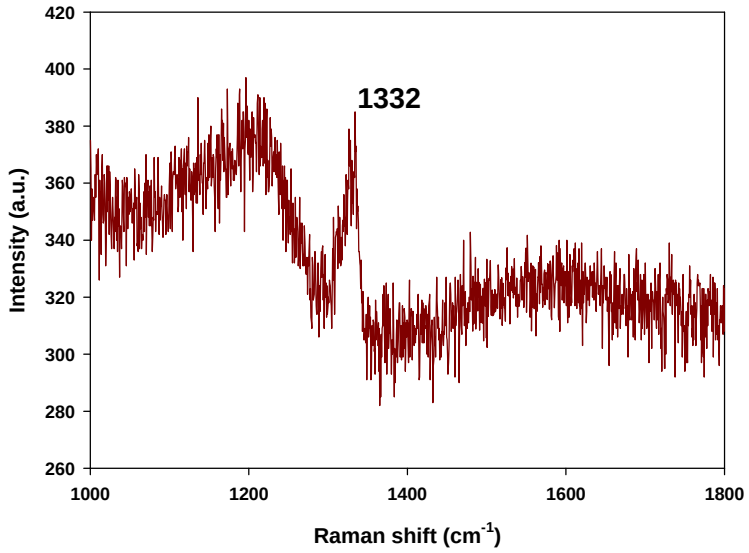

Figure 3-1. Raman spectrum for the BDD electrode

3.2.2. Preparation of a PbO_2 electrode

The PbO_2 electrode was electrodeposited with constant 0.12 A for 2 h in 0.5 M $Pb(NO_3)_2$ + 0.01 M HNO_3 on a Ti mesh substrate that was previously etched in boiling 1.6 M oxalic acid for 2 hr at room tempearture (PbO_2, Ti mesh wire diameter: 0.05 cm, apparent area: 5.5 cm^2) (Da Silva et al. 2010, Mohd and Pletcher 2006). Figure 3-2 shows XRD patterns of the PbO_2 electrode and Ti mesh. As shown in Fig. 3-2, XRD pattern of β-PbO_2 was recognized for the electrodeposited PbO_2 electrode though that of α-PbO_2 was even obtained. Also, no XRD pattern of Ti was obtained for the PbO_2 electrode as compared to XRD pattern for Ti mesh before electrodeposited. A stainless steel mesh was employed as a cathode. This MEA was used in an SPE electrolyzer that consists of an anode and a cathode compartment. The anode compartment is completely separated from the cathode compartment by the MEA.

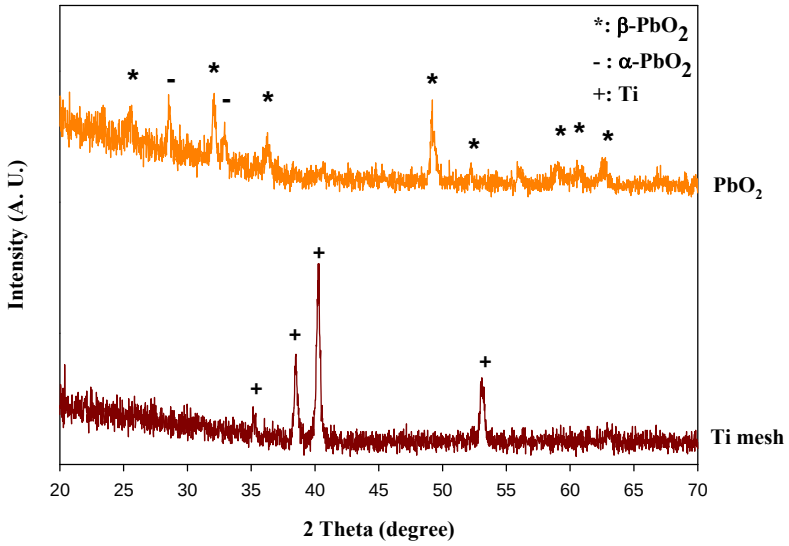

Figure 3-2. XRD patterns of the electrodeposited PbO_2 electrode and a Ti mesh

3.2.3. Preparation of carbon fiber (CF) coated electrode

Figure 3-3 (a) – (b) show scanning electron spectroscopy image of CF and powdered CF. As shown in Fig. 3-3 (a), CF was well produced with the diameter of ~0.3 um, and the specific surface area of the produced carbon fiber was measured at 0.3 g/m^2. In Fig. 3-3 (b), powdered CF seemed to rod shape.

CF produced by an electrospinning method (Lee et al. 2011) was used to prepare a CF-coated stainless steel mesh (CFSS) and a CF-hot-pressed Nafion (CFNA). In the case of CFSS, a mixture of powdered CF and PVDF at a weight ratio of 2:1 with NMP was coated onto a stainless steel mesh substrate (SS 316-mesh, wire diameter: 0.25 mm, apparent area: 5.4 cm^2), and dried for 1 hr at 70^oC (Jeio Tech, FO-600M, Seoul, Korea) (Jang et al. 2005). The coating amount after drying was 17 mg. Powdered CF and PVDF were mixed at a weight ratio of 2: 1 for CFNA, and then a small amount of NMP was continuously added to the mixture until it became clay-like. This mixture was hot-pressed on one side of the Nafion at 25 bar, 100^oC for 1 hr. The amount of loading for CFNA (apparent geometric area: 12 cm^2) was 252 mg. For the H_2O_2 production, a stainless steel mesh counter electrode was used.

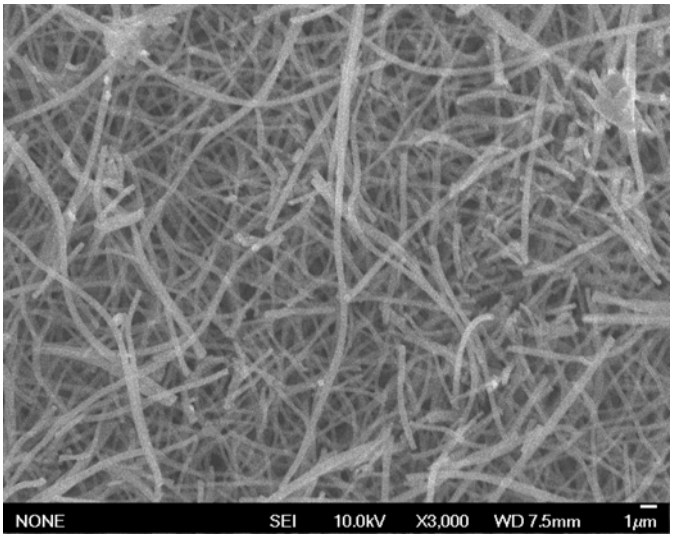

(a)

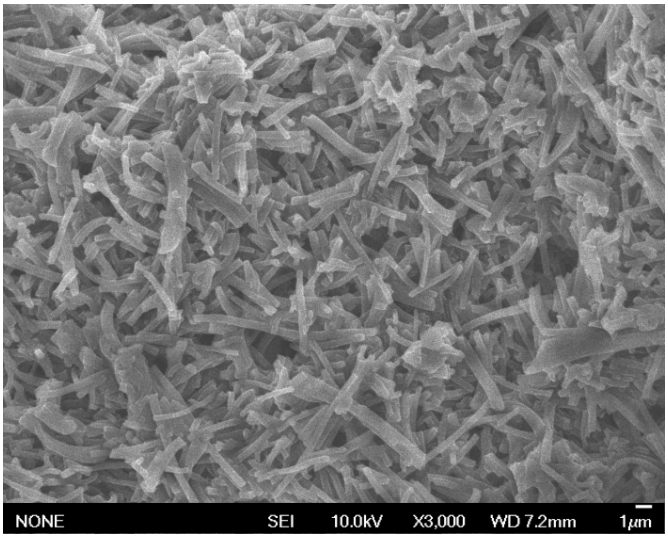

(b)

Figure 3-3. Scanning electron microscope images of (a) electrospinned carbon fiber and (b) powdered carbon fiber

Figure 3-4 (a) and (b) show the schematic cross-sectional views of the two MEAs with the CFSS and CFNA, respectively. As shown in Fig. 3-4 (a) and (b), the MEAs with CFSS (CFSS-MEA) and with CFNA (CFNA-MEA) were composed of their respective working electrodes (CFSS and CFNA), Nafion, and a SS-mesh as a counter electrode that contacted each other. Hydrogen peroxide is produced in the working electrode of these MEAs through the oxygen reduction reaction ($O_2 + 2H^+ + 2e \rightarrow H_2O_2$ at 0.68 V vs. NHE) as water is oxidized to oxygen in the counter electrode ($1/2\ O_2 + 2H^+ + 2e \rightarrow H_2O$ at 1.23 V vs. NHE). An Ag/AgCl electrode was used as a reference, and all potentials in this study are referred to as those vs. Ag/AgCl.

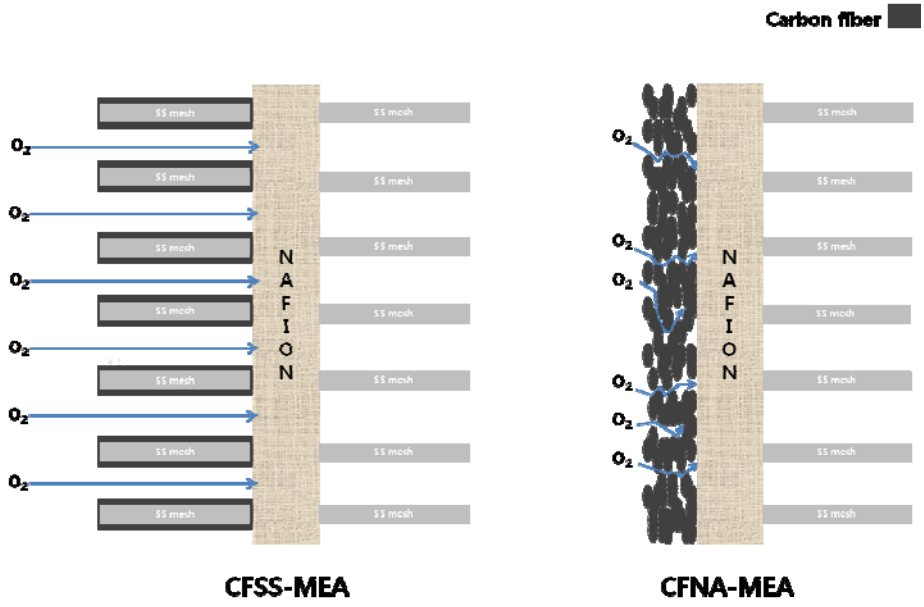

(a) (b)

Figure 3-4. Schematic cross-sectional views of the membrane electrode assembly (a) with the carbon fiber coated stainless steel mesh (CFSS-MEA) and (b) with the carbon fiber hot-pressed Nafion (CFNA-MEA).

3.2.4. Preparation of carbon cloth electrodes

Figure 3-5 shows three types of representative carbon cloth electrodes employed in this study. The first was a carbon cloth electrode without any modification, denoted as CC. The second was a perforated carbon cloth electrode (diameter: 2 mm), denoted as 8PC, 16PC, and 25PC; three numbers, 8, 16, and 25, indicate a number of holes on the electrodes. The last electrode was a stranded carbon cloth electrode, denoted as 1SC, 2SC, 3SC, 5SC, and 10SC**;** the numbers (1, 2, 3, 5, 10) indicate a number of used strands from carbon cloth. Each end of the carbon cloth strands (length: 30 mm) was attached with an electrically conductive adhesive (ELCOAT CX-12, CANS, Japan) on a Ti current collector.

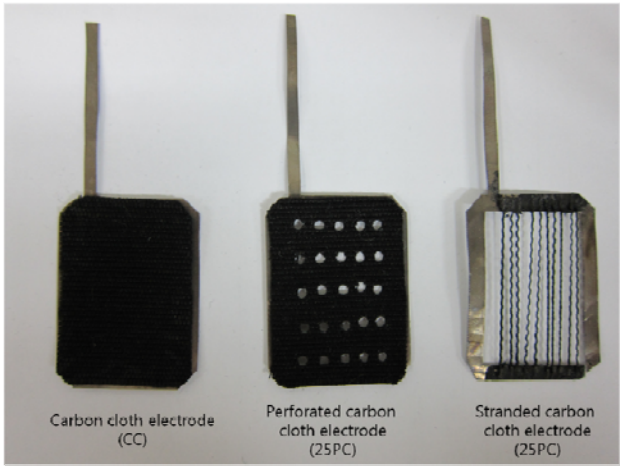

Figure 3-5. Three types of representative carbon cloth electrodes (carbon cloth, perforated carbon cloth, and stranded carbon cloth electrode)

3.3. Electrochemical ROS generation

3.3.1. Electrochemical ozone generation

To examine the production of ozone, EOP was carried out with constant current provided by DC power supply (UDP-150I, Unicorn Tech Co., Seoul, Korea) to a two-electrode system in DW, hydroxyl radical scavengers (t-BuOH or MeOH) (Cho et al. 2005, El-Morsi et al. 2000, Kim and Choi 2002, Sun and Pignatello 1995), or SEs of predetermined concentrations. Then, produced ozone was measured by the indigo method at 600 nm with UV-Vis spectrophotometer (Agilent 8453, Agilent Technologies, Santa Clara, CA, USA) (Bader and Hoigné 1981). Current efficiency of EOP under the various conditions of DW flow rate (Masterflex 7518-00, Cole-Parmer), DW temperature(Model RW-2025G, JEIO TECH, Seoul, Korea) was calculated using Faraday's law (Eq. 3-1) (Awad et al. 2006, Kraft et al. 2006).

$$\text{Current efficiency (\%)} = \frac{VCnF}{i_{app}t} \times 100 \qquad \text{Eq. 3-1}$$

where V is volume of the solution (L), C is the ozone concentration (mol/L), n is the number of electrons required (6), F is the Faraday constant (96,485 C mol^{-1}), i_{app} is the applied current (A), and t is the time (sec).

3.3.2. Electrochemical hydrogen peroxide generation

Carbon fiber coated electrodes-An SPE electrolyzer with the CFSS-MEA or CFNA-MEA in a three-electrode system (Princeton Applied Research, Oak Ridge, TN, USA) was separately employed to examine hydrogen peroxide production. Oxygen (flow rate, 50 mL min^{-1}) was delivered by sparging into the working electrode compartment filled with ultrapure water (75 mL). Chronoamperometry was carried out for predetermined periods (20 min or 3 hr), and cathodic current efficiency and power consumption were calculated using Eq. 3-2 and 3-3.

$$\text{Current efficiency (\%)} = \frac{nFC_{H_2O_2}V}{\int Idt} \times 100\% \qquad \text{Eq. 3-2}$$

$$\text{Power consumption (Wh/g)} = \frac{P\int Idt}{34VC_{H_2O_2}} \times 100\% \qquad \text{Eq. 3-3}$$

where P (V) is applied potential.

Carbon cloth electrodes-All carbon cloth electrodes were cleaned with ultrapure water several times, and air in the electrode pores was removed by vacuum (-0.1 MPa). Then, a Ti current collector, a carbon cloth electrode, Nafion, and stainless steel mesh were placed between the two compartments. Ultrapure water (75 mL) was filled into each compartment. Oxygen was supplied by vigorous mixing (600 rpm). Cyclic voltammetry (CV) and chronocoulometry were carried out in oxygen-saturated ultrapure water that was sparged with oxygen for 30 min prior to experiments. Current densities in CV were obtained from the measured currents, which were divided by the specific surface area multiplied by the mass of the carbon cloth electrode employed. Chronoamperometry was carried out for 20 min at the predetermined applied potential, initial and final hydrogen peroxide concentrations were measured, and then cathodic current efficiency and power consumption, with the current recorded during experiments, were calculated.

3.4. Analysis

3.4.1. Influence of SEs on electrochemical ozone production mechanisms

In order to investigate the influence of SEs on EOP on the BDD electrode, the production of ozone, the formation of •OH, cyclic voltmmetry, and the production of H_2O_2 were examined as a SE varied in types or concentration. EOP was carried out in DW or SEs (0.01 mM, 1 mM, or 100 mM), and 0.020 mM RNO known as an electrochemically inert compound was bleached in the presence or absence of 0.010 mM SEs. Cyclic voltammetry (CV, scan rate: 160 mV/s) was carried out in 0.01 mM and 100 mM SEs as compared to that in DW in a three-electrode system with an Ag/AgCl reference electrode (Potentiostat, Princeton Applied Research, Oak Ridge, TN, USA). H_2O_2 was produced in the presence of 100 mM, 1 mM, and 0.01 mM KH_2PO_4 in comparison with that in DW, and then measured by the DMP method at 454 nm (Baga et al. 1988). H_2O_2 detection was not interfered by O_3.

3.4.2. RNO bleaching for hydroxyl radical formation

For the measurement of the formation of •OH, 0.020 mM RNO known as an electrochemically inert compound was bleached in the presence or absence of 0.010 mM SEs, and the concentration of RNO was measured at 440 nm with UV-Vis spectrophotometer (Comninellis 1994a). Then, the observed first-order rate constant ($k_{RNO,\,obs}$) for the reaction between RNO and •OH was determined by Eq. 3-4 and 3-5 (Cho et al. 2004, Lee and Yoon 2004).

$$-\frac{d[RNO]}{dt} = k_{RNO,^{\bullet}OH}[\bullet OH]_{ss}[RNO] = k_{RNO,obs}[RNO] \quad \text{Eq. 3-4}$$

$$-\ln\frac{[RNO]}{[RNO]_0} = k_{RNO,obs}t \quad \text{Eq. 3-5}$$

where [RNO] is the concentration of RNO, $k_{RNO,\,\bullet OH}$ is the reaction rate constant between •OH and RNO (1.2×10^{10}/M·s) (Buxton et al. 1988), $[\bullet OH]_{ss}$ is the steady state concentration of •OH, and $k_{RNO,\,obs}$ is the $k_{RNO,\,\bullet OH}[\bullet OH]_{ss}$.

3.4.3. p-HBA measurement for hydroxyl radical formation

To investigate the hydroxyl radical formation, 1 mM BA was employed in the reaction, and its hydroxylated product, p-hydroxybenzoic acid (p-HBA), was analyzed (Keenan and Sedlak 2008). p-HBA was measured by UV/high-performance liquid chromatography at 255 nm (UV/HPLC LF13010, Younglin, Seoul, Korea) equipped C18 5 μm column (Agilent, 4.6 × 150 mm). An isocratic elution of 60% acetonitrile and 40% water (pH 2) was employed at a flow rate of 1 mL/min. The standard curve was linear with regression coefficient 0.9999, and the detection limit for p-HBA was 0.0003 mM.

3.4.4. Electrochemical analysis

Cyclic voltammetry (CV, scan rate: 160 mV/s), linear sweep voltammetry (LSV, scan rate: 160 mV s^{-1}) and electrochemical impedance spectroscopy (EIS, at -0.1 V, frequency: 5 Hz - 200 kH) were carried out in a three electrode system with an Ag/AgCl reference electrode (Potentiostat, Princeton Applied Research, Oak Ridge, TN, USA).

Geometric active areas of anodes were determined by the slope of the Anson plot (charge vs. $time^{1/2}$) from the chronocoulometry, as described by Eq. 3-6 (Anson 1966, Cao et al. 2007),

$$Q = 2nFAC_0 \frac{D_0}{\pi^{1/2}} t^{1/2} \qquad \text{Eq. 3-6}$$

where Q is charge (C), A is the geometric active area (cm^2), C_0 is the initial concentration, and D_0 is the diffusion coefficient (cm^2/s). The concentration of DW (C_0) was assumed at 55 mol/cm^3 regardless of the presence of the SEs. The diffusion coefficient of 2.27×10^{-5} cm^2/s was used for DW (Longsworth 1960, Tanaka 1978).

4. Results and discussion

4.1. The suppression of electrochemical ozone production by supporting electrolytes on the BDD electrode

4.1.1. Background

Ozone is an environmental friendly and powerful oxidant because it leaves no harmful byproducts after reaction and exhibits high redox potential (Arihara et al. 2007, Stucki et al. 1985). Due to this, it has a wide variety of applications in disinfection, cleaning, bleaching, wastewater treatment, and water treatment (Onda et al. 2005, Stucki et al. 1987). The most common technology to produce ozone is the corona discharge process with high energy efficiency (~10 Wh/g of Ozone gas). However, this process has several disadvantages such as production of low ozone concentration (~2wt%) and requirement of a cooling system, a drying system, and an ozone diffuser (Cui et al. 2009, Da Silva and Jardim 2006, Da Silva et al. 2003b).

Electrochemical ozone production (EOP) has attracted attention as an alternative technology for water treatment because EOP permits high ozone concentration and direct dissolution of ozone in water, as well as low investment costs (Da Silva et al. 2010, Onda et al. 2005). Electrodes with high oxygen overpotential such as PbO_2 (Amadelli et al. 1999, Da Silva et al. 2006, Da Silva et al. 2010, Tatapudi and Fenton 1993), SnO_2 (Cheng and Chan 2004, Cui et al. 2009, Wang et al. 2005), and boron doped diamond (BDD) electrodes (Arihara et al. 2007, Kraft et al. 2006) were employed as anode materials for EOP.

The presence of inert supporting electrolytes (SEs) in EOP is required to increase the electrical conductivity of water, and facilitate electron transfer between the electrode and the medium as well. It was reported that the nature of SEs is important to determine the efficiency of EOP as PbO_2 electrodes are employed (Babak et al. 1994, Da Silva et al. 2003a, Foller and Tobias 1982). For example, high electronegative anions of SEs such as hexafluorophosphate anions improve current efficiency of EOP on PbO_2 electrodes, showing 3 times more the current efficiency of EOP in comparison with fluoride anions (Foller and Tobias 1982). However, little is known about the role of SEs in EOP on BDD electrodes in spite of several studies on EOP using BDD electrodes(Arihara et al. 2007, Kraft et al. 2006). We investigate the effects of SEs on EOP on a BDD electrode. For this purpose, a solid polymer electrolyte (SPE) electrolyzer permitting deionized water (DW) oxidation even in the absence SEs was employed. EOP was examined in solutions of several inert SEs, and compared to EOP in DW.

Mechanisms for EOP

Since EOP from the electrolysis of water was first reported by Schönbein in the early 1800's (Rubin 2001), the detailed EOP mechanism has been intensively studied. For example, •OH formation, the intermediate for ozone, was investigated during EOP on PbO_2 electrodes(Wabner and Grambow 1985), and adsorbed oxygen species on PbO_2 electrodes was speculated (Foller and Tobias 1982, Kotz

and Stucki 1987). Based on these findings, the commonly accepted mechanism for EOP was suggested as follows (Babak et al. 1994).

$$H_2O \rightarrow (\bullet OH)_{ads} + H^+ + e^- \quad (1)$$

$$(\bullet OH)_{ads} \rightarrow (\bullet O)_{ads} + H^+ + e^- \quad (2)$$

$$(\bullet O)_{ads} + (\bullet O)_{ads} \rightarrow O_2 \quad (3)$$

$$(\bullet O)_{ads} + (O_2)_{ads} \rightarrow O_3 \quad (4)$$

In the case of the PbO_2 electrode, it has been suggested that •OH via oxidation of water (Reaction (1)) is absorbed on the PbO_2 surface, and it facilitates ozone production (Reaction (3) – (4)). In these mechanisms, it has been reported that electrochemical reactions (1) and (2) are kinetic control steps, and chemical reactions (3) and (4) are efficiency control steps (Da Silva et al. 2003a).

In the case of the BDD electrode, it was explained that •OH is weakly bound on the BDD surface due to the inert property of the electrode, resulting that ozone formation on the BDD surface is not favored (Michaud et al. 2003). Also, •OH on the BDD electrode involves the formation of hydrogen peroxide via the combination of •OH (reaction (5)) (Marselli et al. 2003, Michaud et al. 2003).

$$\bullet OH + \bullet OH \rightarrow H_2O_2 \quad (5)$$

4.1.2. Effect of the presence of each individual SE on EOP

Figure 4-1 (a) – (c) show the EOP on the BDD electrode as each individual SE of 100 mM, 1 mM, and 0.01 mM from the five SEs, respectively (KH_2PO_4, KNO_3, $HClO_4$, NaF, and HPF_6 with a current density of 33 $mA \cdot cm^{-2}$) were used and compared with the EOP in DW. As shown in Fig. 4-1, the presence of the SEs (100 mM) brought about an overwhelming suppression of ozone formation when compared with the EOP in DW, regardless of its type. For example, EOP in the presence of SEs was lower by 90 – 99% at 5 min compared to the EOP in DW. In addition, EOP even in the presence of 1 mM (Fig. 4-1 (b)) and 0.01 mM (Fig. 4-1 (c)) SEs was lower by 63 – 80% and 10 – 33% at 5 min, respectively, when compared with that in DW. During EOP, measured potential was summarized in Table S1 in Appendix.

On the other hand, this ozone suppression in the presence of a SE on the BDD electrodes shown in Fig. 1 significantly contrasts with that on the PbO_2 electrode. For example, high electronegative SE anions such as hexafluorophosphate anions rather improved the current efficiency of EOP on the PbO_2 electrodes, showing three times more the current efficiency of EOP when compared with fluoride anions [17].

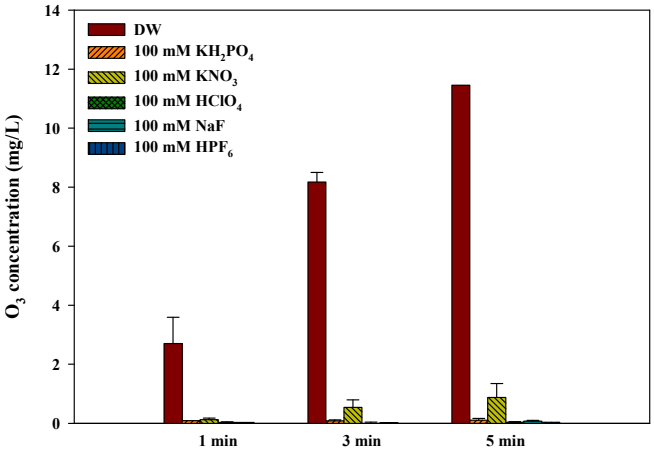
DW
100 mM KH2PO4
100 mM KNO3
100 mM HClO4
100 mM NaF
100 mM HPF6
O3 concentration (mg/L)
0
2
4
6
8
10
12
14
1 min
3 min
5 min

(a)

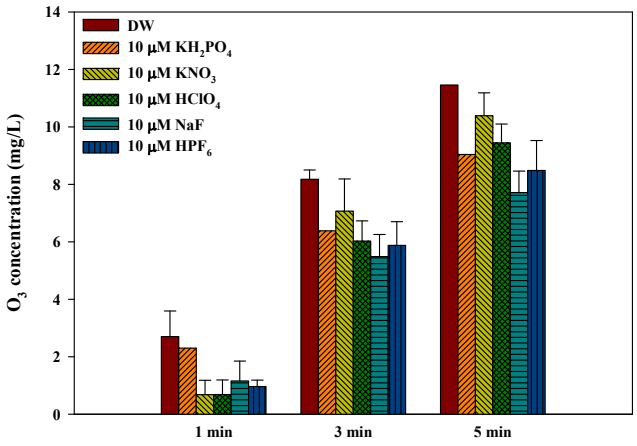
DW
10 μM KH2PO4
10 μM KNO3
10 μM HClO4
10 μM NaF
10 μM HPF6
O3 concentration (mg/L)
0
2
4
6
8
10
12
14
1 min
3 min
5 min

(b)

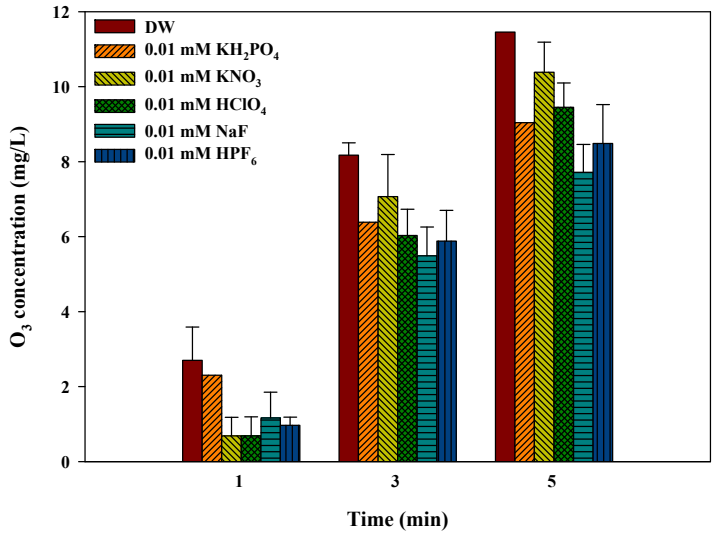

Figure 4-1. Electrochemical ozone production on the boron doped diamond electrode in (a) 100 mM, (b) 1 mM, and (c) 0.01 mM supporting electrolytes as compared with that in DW (supporting electrolytes: KH_2PO_4, KNO_3, $HClO_4$, NaF, and HPF_6, applied constant current: 0.3 A, in the solid polymer electrolyte electrolyzer)

4.1.3. Effect of the presence of each individual SE on ·OH formation

The effect of the presence of each individual SE on the formation of ·OH, which is an intermediate for ozone formation in the EOP process (Reaction (1)), was investigated and was observed from the observed first-order decay rate constants of RNO ($k_{RNO,\ obs}$) in Table 4-1 obtained from Equation (6) in an aqueous solution containing each individual SE at 0.01 mM (KH_2PO_4, KNO_3, $HClO_4$, NaF, and HPF_6 with a constant current of 33 $mA \cdot cm^{-2}$, 30 sec). Since $k_{RNO,obs}$ is the $k_{RNO,\cdot OH}$ $[\cdot OH]_{ss}$ ($k_{RNO,\cdot OH} = 1.2 \times 10^{10}\ M^{-1} \cdot s^{-1}$), the magnitude of $k_{RNO,obs}$ represents the extent of the ·OH formation.

As shown in Table 4-1, the values for $k_{RNO,obs}$ in the presence of each SE were all slightly higher than that in DW, regardless of the type, indicating that at least the presence of a SE does not suppress the formation of ·OH. In addition, in a separate experiment measuring *p*-HBA (hydroxylated product of BA) as an ·OH probe in order to estimate the extent of •OH formation (Fig. 4-2), a similar result to Table 4-1 was obtained.

The observation that the presence of each SE does not suppress the formation of ·OH, but suppresses ozone formation reveals that the oxidation of water to form ·OH (Reaction (1)) is not inhibited by each SE, even at its low concentration while a SE may be involved in interfering with other reactions (Reactions (2) – (4)).

Table 4-1. The observed first-order decay rate constants ($^{a}k_{RNO,obs}$) of the reaction with RNO in aqueous solution containing supporting electrolytes (0.01 mM) compared with that in DW (a constant current of 33 mA·cm^{-2}, 30 sec, the solid polymer electrolyte electrolyzer)

	DW	KH_2PO_4	KNO_3	$HClO_4$	NaF	HPF_6
$k_{RNO,obs}$[a] ($\times 10^{-2}$/s)	3.5 ± 0.1	6.2 ± 0.6	5.7 ± 0.2	5.3 ± 0.8	5.2 ± 0.2	5.5 ± 0.2

a: $k_{RNO,obs}$ is the $k_{RNO,\cdot OH}$ ·$[^{\bullet}OH]_{ss}$, $k_{RNO,\cdot OH}$ is the rate constant between $^{\bullet}OH$ and RNO (1.2×10^{10} M^{-1}·s^{-1}), and $[^{\bullet}OH]_{ss}$ is the steady state concentration of $^{\bullet}OH$.

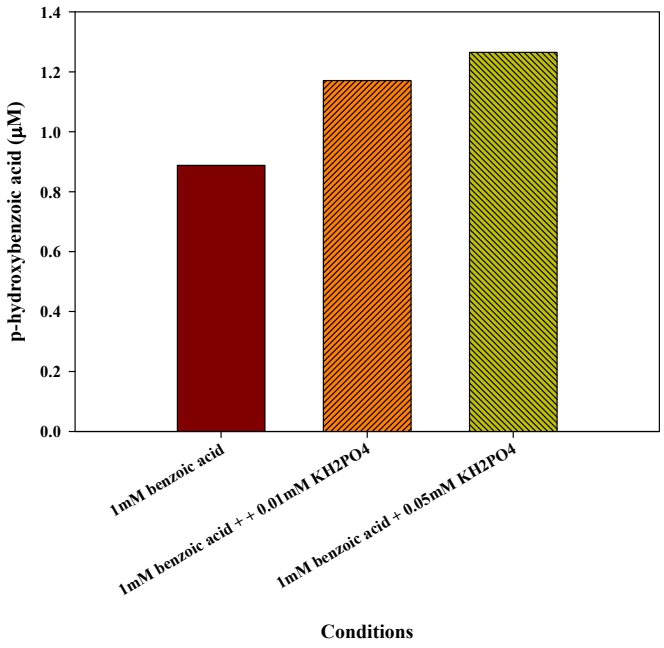

Figure 4-2. The characteristics of •OH formation as expressed by the increase of p-hydorxy benzoic acid (hydroxylated product of benzoic acid (BA)) in the absence and presence of KH_2PO_4 (0.01 mM and 0.05 mM) on boron doped diamond electrode (BDD) (constant current: 111 $mA \cdot cm^{-2}$ for 2 min, the solid polymer electrolyte electrolyzer)

4.1.4. Effect of the presence of each individual SE on oxidation current density in CVs

Figure 4-3 (a) – (e) show the CVs on the BDD electrode in the presence of (a) KH_2PO_4, (b) KNO_3, (c) $HClO_4$, (d) NaF, and (e) HPF_6 (100 mM KH_2PO_4 and KNO_3, scan rate: 160 $mV \cdot s^{-1}$) compared with that in DW (the insets: 0.01 mM of these SEs). This experiment was done to examine the effect of each SE on the electrochemical characteristics of the oxidation of water. As shown in Fig 4-3, in the presence of 100 mM KH_2PO_4 or KNO_3, the extent of anodic current density increased substantially at 2.0 - 3.0 V vs. Ag/AgCl without any significant peak changes. Moreover, the addition of even a low concentration of KH_2PO_4 or KNO_3 (0.01 mM) caused an increase in the anodic current (the insets of Figs. 4-3a and b); the anodic currents for 0.01 mM KH_2PO_4 and KNO_3 at 3 V were 0.71 and 0.67 $mA \cdot cm^{-2}$, respectively, whereas the value for DW was 0.54 $mA \cdot cm^{-2}$. In addition, note that the effect of the other individual SEs on the magnitude of the anodic current density ($HClO_4$, NaF, and HPF_6) represented similar CV trends.

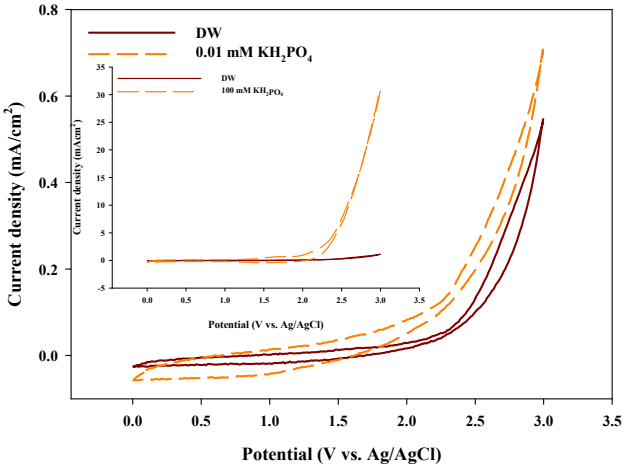
DW
0.01 mM KH2PO4
DW
100 mM KH2PO4
Current density (mA/cm2)
Potential (V vs. Ag/AgCl)

(a)

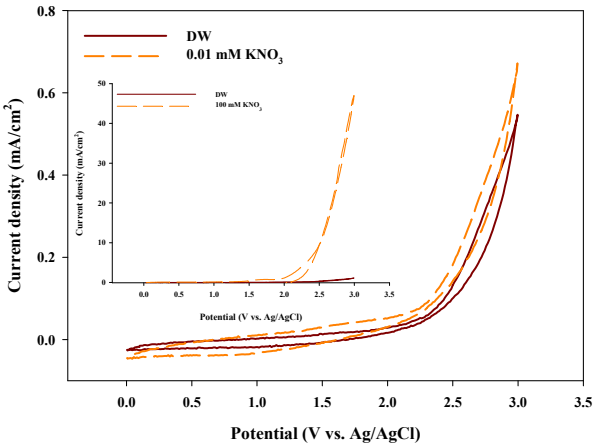
DW
0.01 mM KNO3
DW
100 mM KNO3
Current density (mA/cm2)
Potential (V vs. Ag/AgCl)

(b)

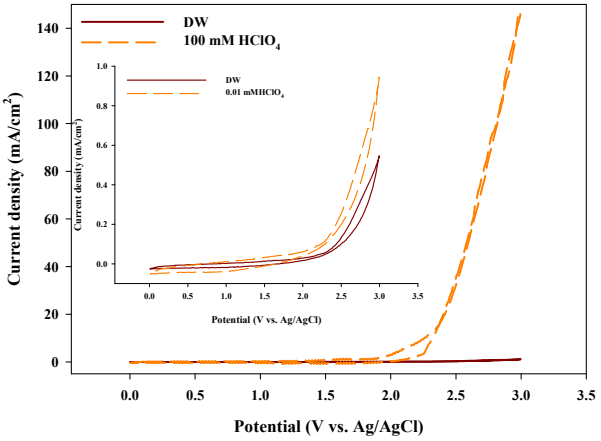
DW
100 mM HClO4
Current density (mA/cm2)
Potential (V vs. Ag/AgCl)
DW
0.01 mMHClO4
Current density (mA/cm2)
Potential (V vs. Ag/AgCl)

(c)

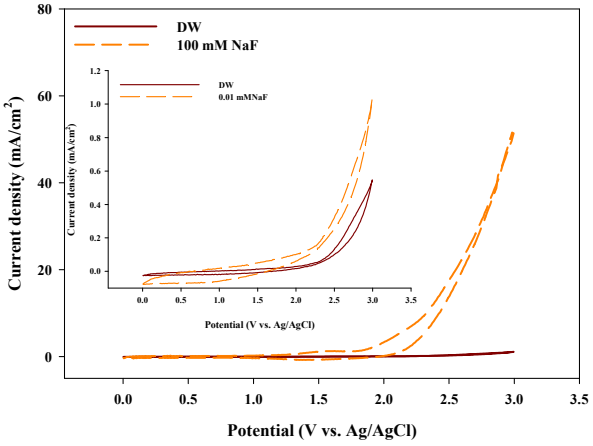
DW
100 mM NaF
Current density (mA/cm2)
Potential (V vs. Ag/AgCl)
DW
0.01 mMNaF
Current density (mA/cm2)
Potential (V vs. Ag/AgCl)

(d)

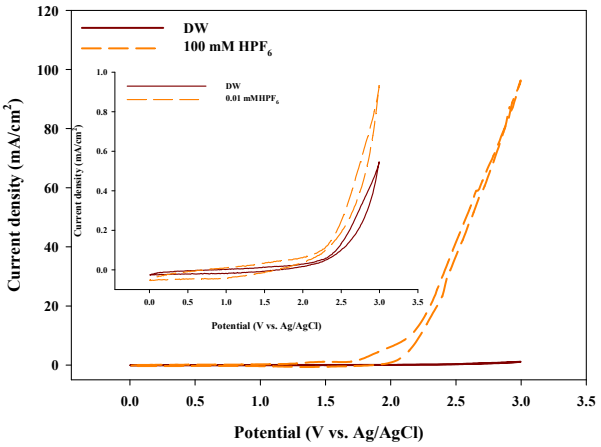

(e)

Figure 4-3. CVs on the boron doped diamond (BDD) electrode in (a) 100 mM KH_2PO_4 and (b) KNO_3 compared with that in DW (inset: 0.010 mM KH_2PO_4 and KNO_3, scan rate: 160 $mV \cdot s^{-1}$, in the solid polymer electrolyte electrolyzer)

In addition, the $^{\bullet}O$ formation was investigated with the Tafel plots (Fig. S4) as previously examined (Babak et al. 1994). The slopes of the plots were not changed with the addition of the SEs (KH_2PO_4 and KNO_3). This indicates that reaction (2) was not inhibited.

The increase in $^{\bullet}OH$ formation (Table 4-1) and the anodic currents (Fig. 4-3) in the presence of the SEs indicates that Reactions (1) and (2) are possibly not hindered by the SEs. In addition, they can be attributed to increased reaction sites because water oxidation in the absence of the SEs in the SPE electrolyzer occurs only along the three phase boundary, which is the intersection of the Nafion-H electrolyte (liquid-like phase), the electrodes (solid), and the water (liquid) [1, 36, 37], whereas in the presence of the SEs, it can take place on all the electrode surfaces including the three phase boundary. Accordingly, ozone suppression in the presence of the SEs suggests that other chemical reactions such as the combination of $^{\bullet}O$ (Reaction (3)) and reaction of $^{\bullet}O$ with O_2 (Reaction (4)) can be inhibited by the SEs.

4.1.5. Effect of SEs on hydrogen peroxide production

In order to investigate the effect of SEs on the production of hydrogen peroxide which is generated via the combination of $^{\bullet}OH$ (Reaction (5)) and through EOP, the electrochemical production of hydrogen peroxide (Fig. 4-4 (a)) and ozone (Fig. 4-4 (b)) on the BDD electrode was examined as the KNO_3 concentration was varied from 0.01 mM to 100 mM (with a current density of 33 $mA \cdot cm^{-2}$). As shown in Fig. 4-4, the higher the SE concentration was, the larger the reduction of hydrogen peroxide and ozone was. For example, hydrogen peroxide production in 100 mM, 1 mM, and 0.01 mM KNO_3 decreased by 98%, 83%, and 25% at 5 min, respectively, compared to that in DW (Fig. 4-4 (a)). Moreover, EOP in 100 mM KNO_3 was almost negligible (98% decrease) and that in 1 mM and 0.01 mM KNO_3 decreased by 83% and 25% at 5 min compared to that in DW, respectively (Fig. 4-4 (b)). In a separate experiment investigating the effect of KH_2PO_4 on the production of hydrogen peroxide (Fig. 4-5 (a)) and ozone production (Fig. 4-5 (b)) similar results to the ones in Fig. 4-4 were observed.

The decrease in hydrogen peroxide formation shown in Fig. 4-4 (a) can be interpreted as the combination of $^{\bullet}OH$ being hindered by the SEs because $^{\bullet}OH$ formation is not disturbed even at a low concentration for the SEs (Table 4-1). In a similar manner, the suppression of EOP by the SEs can be explained by hindering the combination of $^{\bullet}O$ (Reaction (3)).

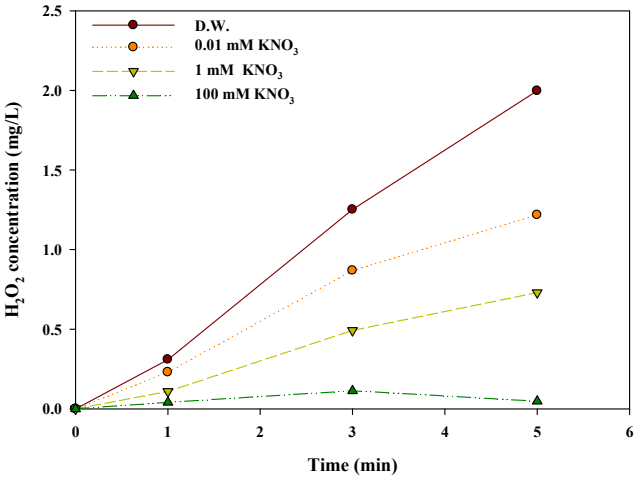

(a)

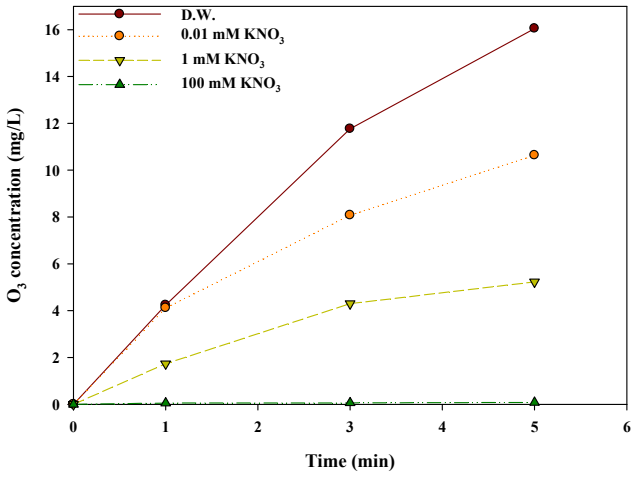

(b)

Figure 4-4. Electrochemical production of (a) hydrogen peroxide and (b) ozone on the boron doped diamond (BDD) electrode in the presence of KNO_3 (0.01 mM, 1 mM, and 100 mM) compared with that in DW (33 $mA \cdot cm^{-2}$, the solid polymer electrolyte electrolyzer)

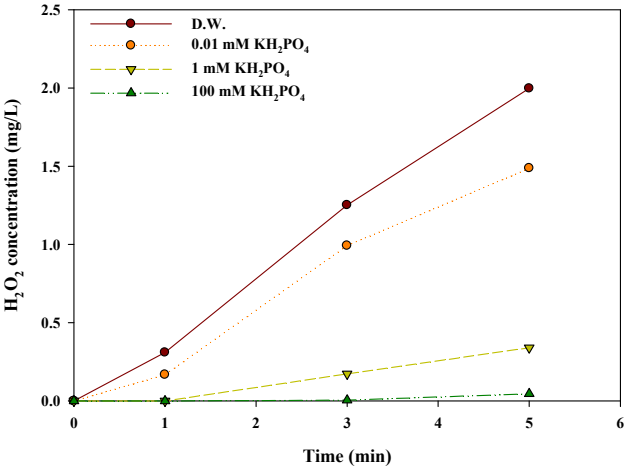

(a)

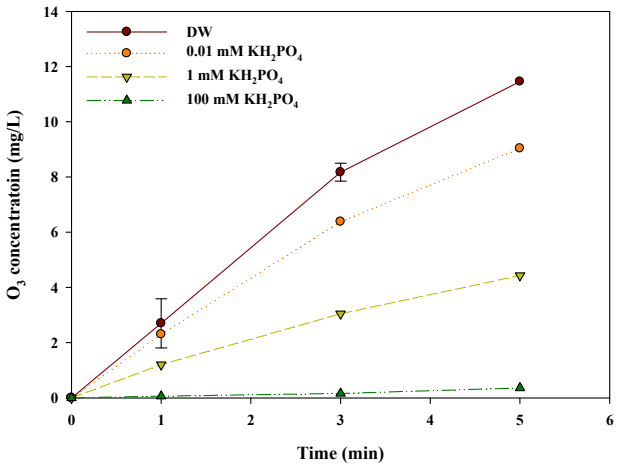

(b)

Figure 4-5. Electrochemical production of (a) hydrogen peroxide and (b) ozone on the boron doped diamond (BDD) electrode in the presence of KH_2PO_4 (0.01 mM, 1 mM, and 100 mM) compared with that in DW (33 $mA \cdot cm^{-2}$, the solid polymer electrolyte electrolyzer)

4.1.6. Mechanisms responsible for the suppression of EOP by the SEs

Based on the results in Figs. 4-1 – 4-5 and Table 4-1, the reaction scheme of EOP suppression in the presence of the SEs on the BDD electrode is illustrated in Fig. 4-6. Note that the SEs caused the suppression of EOP (Fig. 4-1), enhanced the $^{\bullet}$OH formation (Table 4-1) and anodic current of CV (Fig. 4-3) and reduced hydrogen peroxide formation (Fig. 4-4). As shown in Fig. 4-6, the inert SE anions on the BDD surface could physically interfere with the diffusion or combination of $^{\bullet}$O, resulting in decreases in the ozone production and, instead, probably increases in oxygen evolution. This is because an electrical double layer forms on the electrode surface once an electrical potential is applied to the electrode [38]. For example, EOP at a high concentration of SE (Fig. 4-6 (a)) could cause more interference than that at a low concentration of SE (Fig. 4-6 (b)) because the SE anions are densely packed onto the surface with a high concentration of SE more so than at a low concentration of SE. On the other hand, $^{\bullet}$O on the BDD surface in DW (Fig. 4-6 (c)) could diffuse to the bulk, and react with the adjacent $^{\bullet}$O without interference from the presence of the SE anions.

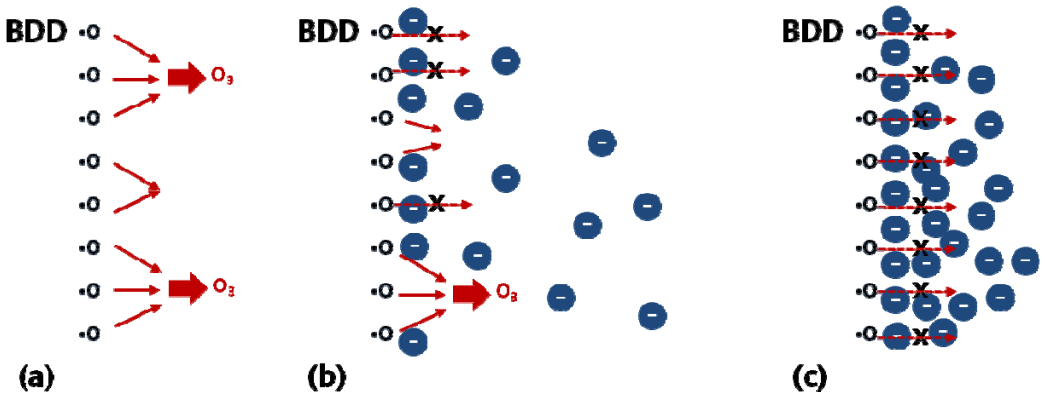

Figure 4-6. The reaction scheme suggested for explaining the suppression of electrochemical ozone production (EOP) in the presence of a supporting electrolyte (SE) on the boron doped diamond electrode (BDD) at (a) a high concentration of the SE, (b) a low concentration of the SE, and (c) DW

4.1.7. Conclusions

In this study, the influence of SEs in EOP on a BDD electrode was investigated. The presence of SEs led to a significant suppression of EOP on the BDD electrode. $^{\bullet}OH$ formation and anodic currents in CVs were not inhibited by the presence of even a low concentration of SEs, but the production of hydrogen peroxide was suppressed by the presence of SE on the BDD, indicating that the SE hinders the combination of $^{\bullet}OH$. Based on these findings, a mechanism of EOP suppression in the presence of a SE is suggested. The suppression of EOP on the BDD electrode can be explained by the interference of the diffusion or combination of $^{\bullet}O$ by the SE anions locally concentrated on the electrode surface by electrostatic attraction.

4.2. Operating conditions for high yield EOP

4.2.1. Background

Ozone with high oxidation power is environmental friendly due to no residuals after reaction (Arihara et al. 2007, Stucki et al. 1985). Due to this, it is employed in many fields such as a cleaning agent of food industries, a bleaching agent of textile and wood pulp, or an oxidant in water or wastewater treatment (Onda et al. 2005, Stucki et al. 1987). The Corona process is widely used for on-site generation of ozone, but this process restricts application of using high concentrated ozone (corona process: 2 wt%) (Cui et al. 2009, Da Silva et al. 2003b). One of candidates to circumvent the restriction is electrochemical ozone production (EOP).

Since EOP allows generating high concentration ozone as well as direct dissolution of ozone in water (Da Silva et al. 2010, Onda et al. 2005), EOP has attracted attention for water treatment. Lead dioxide (PbO_2) electrodes (Amadelli et al. 1999, Da Silva et al. 2006, Da Silva et al. 2010, Tatapudi and Fenton 1993) and boron doped diamond (BDD) electrodes (Arihara et al. 2006, Arihara et al. 2007, Kraft et al. 2006) are considered as anode materials for EOP ($O_3 + 6H^+ + 6e = 3H_2O$ at 1.51 V vs. NHE). On these electrodes, operating conditions such as flow rate, temperature, and applied current render current efficiency of EOP diverse.

Figure 4-7 shows current efficiency of EOP on BDD and PbO_2 electrodes in the

literature (Arihara et al. 2006, Arihara et al. 2007, Da Silva et al. 2006, Da Silva et al. 2010, Foller and Goodwin 1984, Kraft et al. 2006, Nishiki et al. 2011, Onda et al. 2005, Stucki et al. 1987, Stucki et al. 1985, Tatapudi and Fenton 1993). As shown in Fig. 1, current efficiency of EOP on BDD and PbO_2 electrodes varied under different conditions. For example, the current efficiency of EOP on the BDD electrodes was achieved in the range of 13 – 47%, and that for PbO_2 remained at 5 – 35%. Although many studies reported EOP under various operating conditions, little is known for electrical conductivity, which represents water quality in a fast and reliable way, affecting EOP.

The aim of this study is to investigate electrical conductivity of solution for optimal yield EOP. EOP was performed in a solid polymer electrolyte (SPE) electrolyzer that permits oxidation of ultrapure water (UPW) even without supporting electrolytes (SEs) as the operating conditions of electrical conductivity, anodes (BDD and PbO_2), flow rate, temperature, and applied current varied.

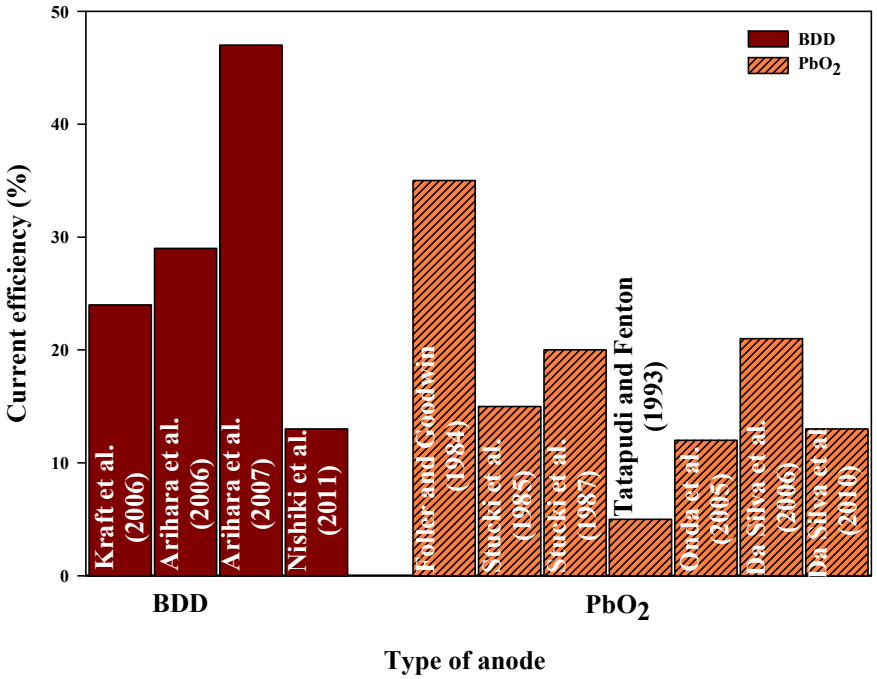

Figure 4-7. Current efficiency of electrochemical ozone production on BDD and PbO_2 electrodes

4.2.2. Influence of electrical conductivity of solution on the BDD and PbO_2 electrode

Figure 4-8 show the influence of type of water on electrochemical ozone production (EOP) on the (a) boron doped diamond (BDD) and (b) PbO_2 electrode, respectively. As shown in Fig. 4-8, using tap water and pure water lowered EOP rate on both electrodes as compared to ultrapure water in EOP rate. For example, the rates on BDD electrode appeared to decrease by 70% as compared to that using UPW. Even using pure water (0.055 $mS \cdot cm^{-1}$), the production rate was reached to only 56% in comparison with UPW. On the PbO_2, the rates in the tap water and pure water decreased by 50% and 18%, respectively. The trend of EOP decreases on the BDD is consistent with previous results that using tap water lowered ozone production rate on a BDD electrode as compared to the ozone production rate in pure water (Nishiki et al. 2011) and electrical conductivity of solutions lowered the current efficiency of EOP on a BDD electrode (Kraft et al. 2006)

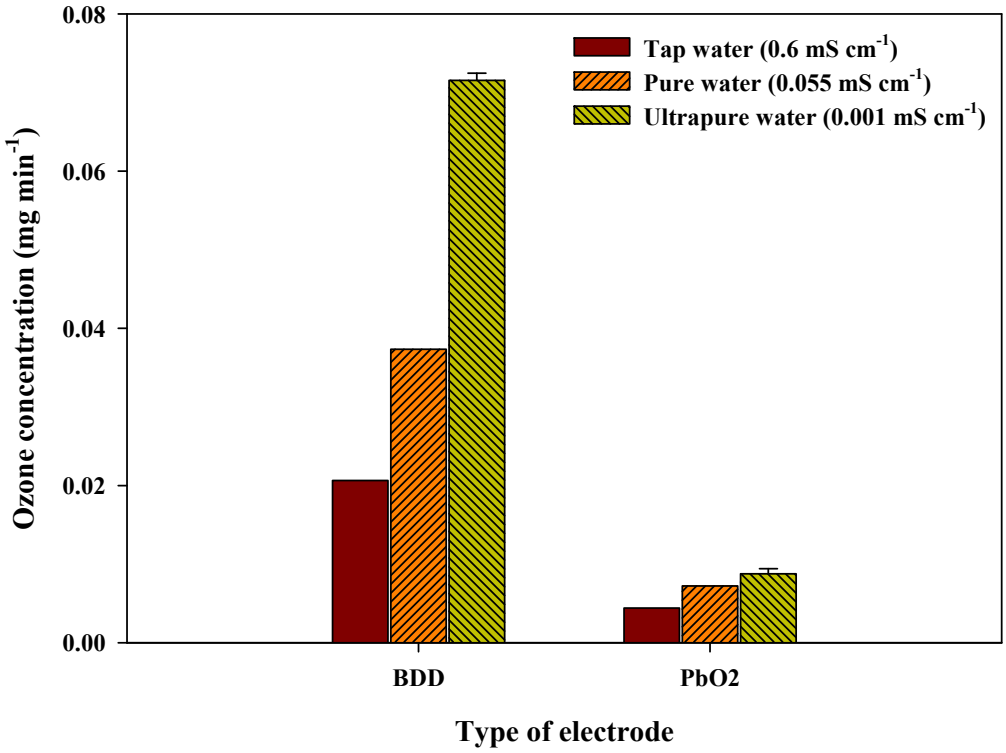

Figure 4-8. Influence of type of water on electrochemical ozone production (EOP) rate on the boron doped diamond and PbO_2 electrode (Ultrapure water: 0.001 mS·cm^{-1}, 0.055 mS·cm^{-1}, 0.6 mS·cm^{-1}, electrolysis time: 5 min, applied constant current: 0.3 A, in the solid polymer electrolyte electrolyzer without the flow rate at 20℃)

Figure 4-9 shows the influence of electrical conductivity on EOP on the BDD and PbO_2 electrode as the electrical conductivity of solution containing KH_2PO_4 varied from 0.001 $mS \cdot cm^{-1}$ (UPW) to 30 $mS \cdot cm^{-1}$ (applied constant current: 0.3 A, electrolysis time: 10 min, without flow at 20℃ in the SPE electrolyzer). As shown in Fig. 4-9, EOP was reduced on the BDD electrode with increasing the electrical conductivity from 0.001 (UPW) to 30 $mS \cdot cm^{-1}$, but that on the PbO_2 electrode fluctuated between 0.4 and 30 $mS \cdot cm^{-1}$. For example, EOP on the BDD electrode at 0.008, 0.4, and 30 $mS \cdot cm^{-1}$ decreased by 25, 67, 99%, respectively, as compared that at 0.001 $mS \cdot cm^{-1}$. On the contrary, EOP on the PbO_2 at 0.08 and 0.4 $mS \cdot cm^{-1}$ decreased by 20 and 36 %, respectively, but that at 30 $mS \cdot cm^{-1}$ was recovered up to 96% in comparison with that at 0.001 $mS \cdot cm^{-1}$. Figure 4-9 reveals that effective electrodes for EOP depends on electrical conductivity of solution (EOP at 0.001 – 0.4 $mS \cdot cm^{-1}$: BDD > PbO_2, EOP at 30 $mS \cdot cm^{-1}$: BDD < PbO_2).

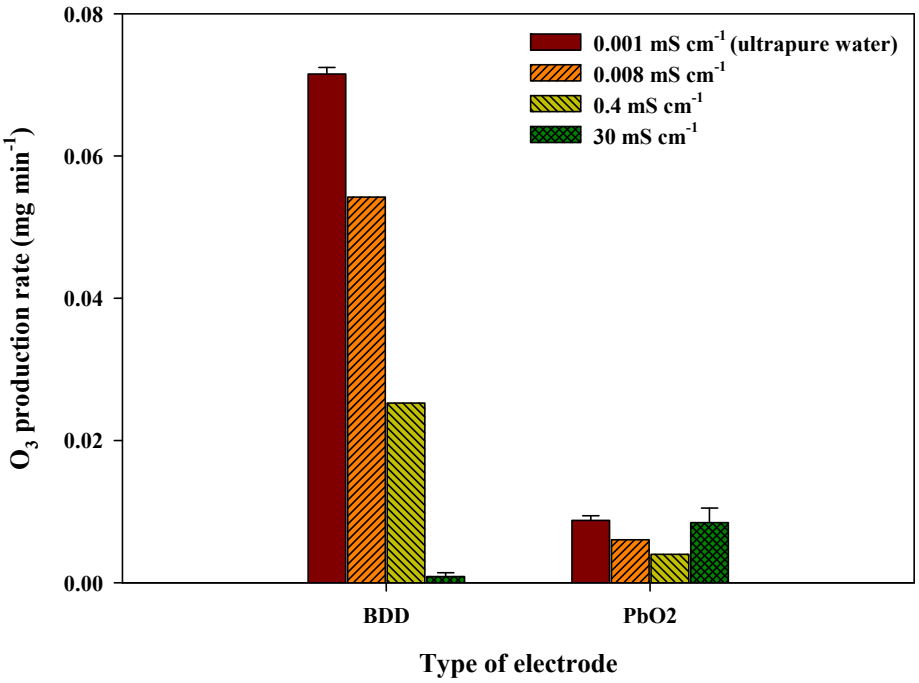

Figure 4-9. Influence of electrical conductivity of solution containing KH_2PO_4 on electrochemical ozone production (EOP) rate on the boron doped diamond (BDD) and PbO_2 electrode (KH_2PO_4 concentration: 0.01, 1,and 100 mM, applied constant current: 0.3 A, electrolysis time: 10 min, in the solid polymer electrolyte electrolyzer without the flow rate at 20℃)

4.2.3. Relationship between EOP rate on the BDD electrode and electrical conductivity of solution

In order to investigate relationship between ozone production rate on the BDD electrode and electrical conductivity of solution, the rates were plotted as the electrical conductivity (or TDS) obtained from solution containing each SE (KH_2PO_4, KNO_3, $HClO_4$, NaF, and HPF_6) varied from 0.001 mS·cm (UPW) to 30 $mS \cdot cm^{-1}$ in the SPE electrolyzer (Fig. 4-10). As shown in Fig. 4-10, the rates were linear with reverse log-electrical conductivity of solutions ($r^2 = 0.98$). For example, at high electrical conductivity, the ozone production rate was almost negligible, but at low electrical conductivity, the ozone production rate was obtained at 0.08 $mg \cdot min^{-1}$.

In addition, ozone production rates on the BDD and the capacitance measure in CV (scan rate: 160mV/s) were investigated in Fig. S3 in Appendix, and the rates were linear with reverse log-capacitance ($r^2 = 0.98$).

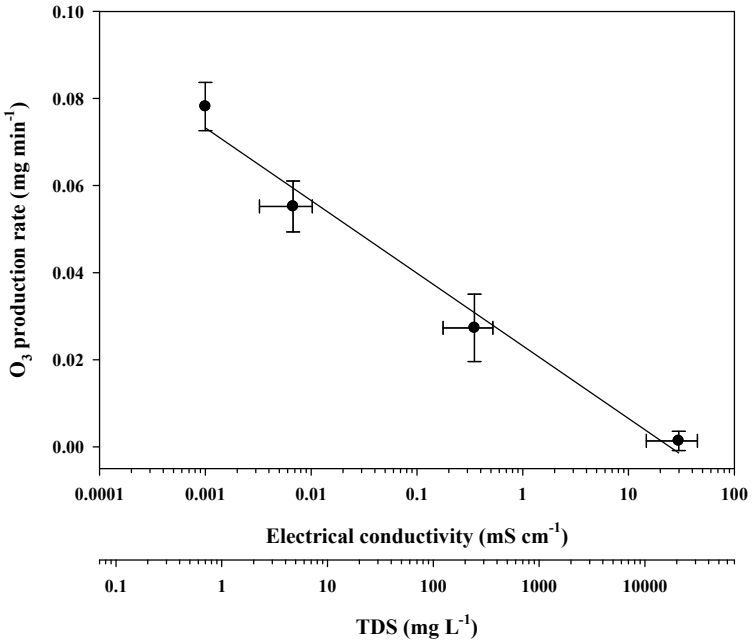

Figure 4-10. Relationship between ozone production rate on the boron doped diamond (BDD) electrode and electrical conductivity of solution containing each supporting electrolyte (SE) from 0.001 to 40 $mS \cdot cm^{-1}$ (SE: KH_2PO_4, KNO_3, $HClO_4$, NaF, and HPF_6, applied constant current: 0.3 A, electrolysis time: 10 min, in the solid polymer electrolyte electrolyzer without the flow rate at 20℃)

From the results of Fig. 4-10, different efficacies of EOP on BDD electrodes can be expected for the different type of solutions. For example, in the case of UPW, optimal yield EOP can be achieved on the BDD electrodes. In the solution of higher electrical conductivity than UPW, lower efficacies of EOP would be inevitable. In order to achieve high yield EOP, electrical conductivity of solution should be lowered by pretreatments such as capacitive deionization in the consideration of cost effectiveness of such treatments. In addition, very low electrolyte-contained water (~6 $\mu S \cdot cm^{-1}$) generated from fuel cell processes (Tibaquirá et al. 2011) can be considered as the water for EOP. In the case of high electrical conductivity of solution (>30 $mS \cdot cm^{-1}$), employing PbO_2 electrodes would be effective for EOP rather than employing BDD electrodes (Fig. 4-9).

4.2.4. Electrochemical properties of the BDD and PbO_2 electrode

In order to examine electrochemical properties of the BDD and PbO_2 electrode in UPW, the formation of $^{\bullet}OH$ expressed by the observed first-order decay rate constants of RNO ($k_{RNO,\,obs}$) (constant current of 33 $mA \cdot cm^{-2}$, 30 sec), geometric active area obtained from the Anson plot (potential step: 0 to 2 V vs. Ag/AgCl), and oxygen overpotential measured from LSV were investigated without flow at 20℃ in the SPE electrolyzer (Table 4-2). As shown in Table 4-2, all the electrochemical properties for the BDD electrode were outperformed more than those for the PbO_2 electrode. For example, the rate constant and geometric active area for the BDD electrode were almost 3 times higher than those for the PbO_2. Note that $k_{\mathrm{RNO,obs}}$ is the $k_{RNO,^{\cdot}OH}$ $[^{\bullet}OH]_{ss}$ ($k_{RNO,^{\cdot}OH} = 1.2 \times 10^{10}$ $M^{-1} \cdot s^{-1}$),so the magnitude of $k_{RNO,obs}$ represents the extent of the $^{\bullet}OH$ formation. Moreover, oxygen overpotential for the BDD was at 0.3 V higher. The BDD electrode generating hydroxyl radical more than the PbO_2 electrode is in accordance with the previous explanation that electrochemical oxidation of pollutants for BDD electrodes was efficient due to more hydroxyl radical generation for BDD electrodes than PbO_2 electrodes (Martínez-Huitle et al. 2008, Panizza and Cerisola 2007, 2008, Sirés et al. 2008, Weiss et al. 2008, Weiss et al. 2006). Also, the high oxygen overpotential of the BDD electrode is in consistent with previous results (Da Silva et al. 2003b, Kapałka et al. 2008).

The better performance of EOP on the BDD electrode in UPW can be attributed to fast hydroxyl radical (the intermediate for EOP) production, large geometric active area, and high oxygen overpotential as compared to the PbO_2 electrode (Table 4-2).

Table 4-2. The observed first-order decay rate constants ($k_{RNO,obs}$) measured by RNO bleaching (constant current of 33 mA·cm^{-2}, 40 s), geometric active area measured from Anson plot (potential step: 0 to 2 V vs. Ag/AgCl), and oxygen overpotential measured from linear sweep voltammetry (LSV) (scan rate: 160 mV ·s) on a boron doped diamond (BDD) electrode in deionized water in comparison with that on a PbO_2 electrode

	BDD	PbO_2
$k_{RNO,obs}$ [a] (× 10^{-2}·s^{-1})	4.1	0.56
Geometric active area (× 10^{-4} cm^2)	1.0	0.34
Oxygen overpotential (V)	2.0	1.7

a: $k_{\mathrm{RNO,\,obs}}$ is the $k_{RNO,\,\cdot OH}$ $[^{\bullet}\mathrm{OH}]_{ss}$ ($k_{RNO,\,\cdot OH}$ is the rate constant between $^{\bullet}$OH and RNO (1.2 × 10^{10} M^{-1}·s^{-1}), and $[^{\bullet}\mathrm{OH}]_{ss}$ is the steady state concentration of $^{\bullet}$OH.

Figure 4-11 shows the influence of 300 mM hydroxyl radical scavengers on EOP rate on the BDD and PbO_2 electrode at 0.001 $mS \cdot cm^{-1}$ (UPW) as compared to EOP without the scavengers (the scavengers: t-BuOH and MeOH, applied constant current: 0.3 A, electrolysis time: 5 min, in the SPE electrolyzer without flow at 20℃). As shown in Fig. 4-11, EOP rates on the BDD electrode were negligible in both 300 mM t-BuOH and MeOH, but the considerable rates were observed on the PbO_2 electrode even with both scavengers. For example, the rates on the PbO_2 electrode with t-BuOH and MeOH were measured at 0.005 and 0.002 $mg \cdot min^{-1}$, respectively.

The result of Fig. 4-11 is believed to indicate the extent of hydroxyl radical adsorption on the electrode surface. For example, it can be interpreted that hydroxyl radical is weakly adsorbed on the BDD surface (Michaud et al. 2003), so that both t-BuOH and MeOH scavenged all the hydroxyl radical, resulting in no ozone production. In contrast, it can be interpreted that weakly and strongly adsorbed hydroxyl radical coexists on the PbO_2, so that strongly adsorbed hydroxyl radical is not scavenged by both t-BuOH and MeOH, resulting in a certain extent of ozone production. With this presumption, at low electrical conductivity (0.001 – 0.4 $mS \cdot cm^{-1}$), EOP would be suppressed by SEs in the consideration of the previous explanation (Section 4.1), resulting in EOP decreases. However, at high electrical conductivity, electronegativity of SEs

dominantly facilitated EOP (Foller and Tobias 1982), so EOP was recovered.

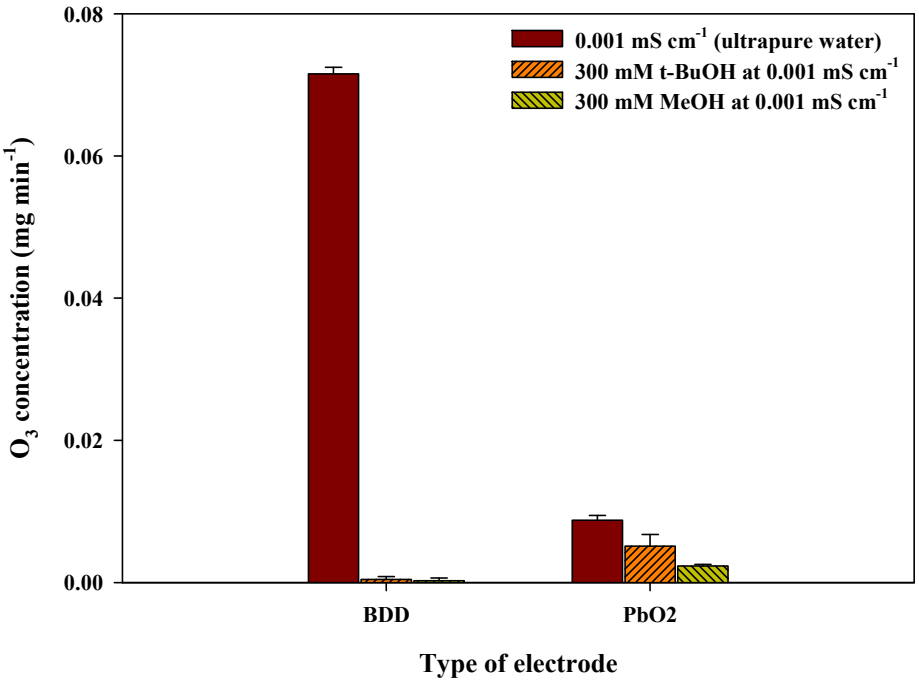

Figure 4-11. Influence of hydroxyl radical scavengers on electrochemical ozone production (EOP) rates on the boron doped diamond (BDD) and PbO_2 electrode (the scavengers: 300 mM t-BuOH and MeOH, applied constant current: 0.3 A, electrolysis time: 10 min, in the solid polymer electrolyte electrolyzer without the flow rate at 20℃)

4.2.5. Influence of flow rate, temperature, and applied current on EOP on the BDD and PbO_2 electrode

Since flow rate, temperature, and applied current significantly affects EOP, the influence of these conditions on current efficiency of EOP on the BDD and PbO_2 electrode (Fig. 4-12) was investigated at 0.001 $mS \cdot cm^{-1}$ (UPW) as flow rate, temperature, and applied current varied (UPW flow rate: 0, 100, and 200 $mL \cdot min^{-1}$, UPW temperature: 4 and 20℃, applied constant current: 0.3, 0.5, and 1 A in the SPE electrolyzer). As shown in Fig. 4-12, the conditions of fast flow rate of UPW, high applied current, and low temperature of UPW enhanced the current efficiency of EOP on both electrodes. For example, the highest current efficiency on the BDD was found at 14% (200 $mL \cdot min^{-1}$, 4℃, 1 A) that was 5 times higher than that on the batch condition (no flow at 20℃). Also, the current efficiency of EOP on the PbO_2 was achieved at 4% (200 $mL \cdot min^{-1}$, 4℃, 1 A) even though that of 0.3% was measured at batch condition. The trend of increases in EOP under the condition of fast flow rate of UPW, high applied current, and low temperature of UPW was in accordance with the previous publications (Cui et al. 2009, Da Silva et al. 2006, Kraft et al. 2006).

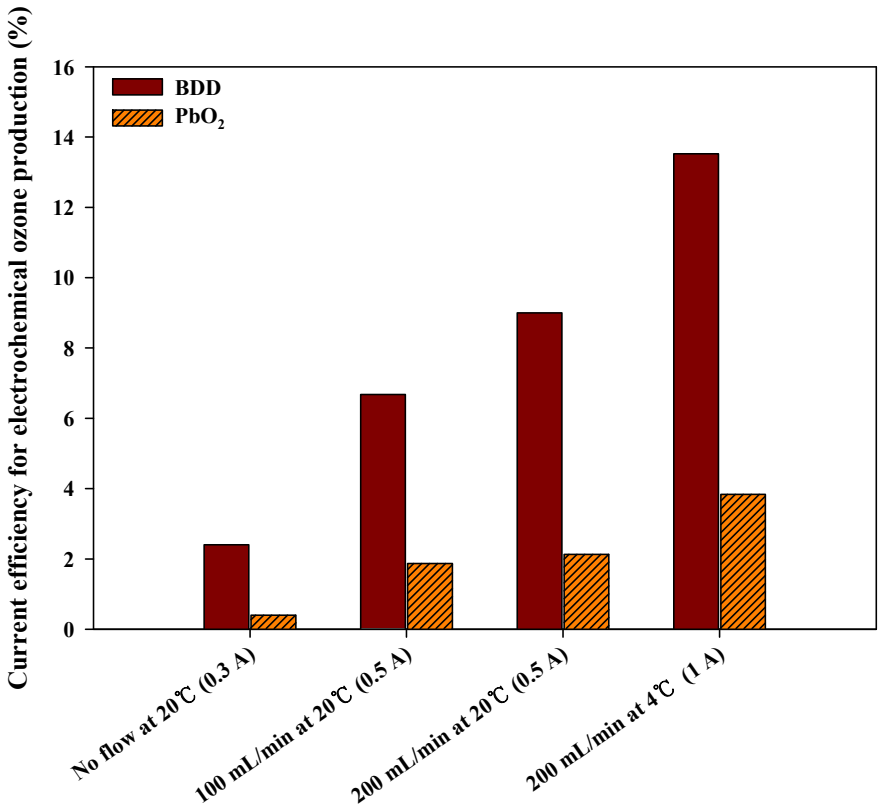

Figure 4-12. Effect of the operating conditions of ultrapure water (UPW) flow rate, temperature, and applied current on current efficiency of electrochemical ozone production (EOP) on the boron doped diamond (BDD) and PbO_2 electrode (UPW flow rate: 0, 100, or 200 mL·min, UPW temperature: 20℃ or 4℃, applied constant current: 0.3 A, 0.5 A, or 1 A, in the solid polymer electrolyte electrolyzer)

4.2.6. Conclusions

We investigated electrical conductivity of solution for optimal yield EOP. Low electrical conductivity (0.001 $mS \cdot cm^{-1}$) led to effective EOP; high current efficiency (~14 %) of EOP was achieved on the BDD electrode under the conditions of 1A and 200 $mL \cdot min^{-1}$ 4℃ as compared to that on the PbO_2 electrode (4%). However, increasing electrical conductivity of solutions from 0.001 to 30 $mS \cdot cm^{-1}$ linearly reduced EOP on the BDD while EOP on the PbO_2 electrode was slightly decreased with the conductivity from 0.001 to 0.4 $mS \cdot cm^{-1}$, and then recovered at 30 $mS \cdot cm^{-1}$. At low electrical conductivity (0.001 – 0.4 $mS \cdot cm^{-1}$), BDD electrodes would allow high yield EOP, but PbO_2 electrodes would become effective at high electrical conductivity for EOP (> 30 $mS \cdot cm^{-1}$).

4.3. High yield hydrogen peroxide production in a solid polymer electrolyte electrolyzer with a carbon fiber coated mesh substrate

4.3.1. Background

Hydrogen peroxide is an environmentally friendly oxidant because it leaves no harmful chemicals after reacting and has been used in many fields such as pulp bleaching, textiles, and advanced oxidation processes (Murayama and Yamanaka 2011, Qiang et al. 2002). An anthraquinone process is generally employed to produce hydrogen peroxide, but this process has several disadvantages such as high operating cost and concerns about transporting and handling concentrated hydrogen peroxide (Gallegos et al. 2005, Lobyntseva et al. 2007). For these reasons, an on-site and energy efficient system for generating hydrogen peroxide is necessary.

An electrochemical system is an attractive candidate to generate hydrogen peroxide through oxygen reduction, and several types of electrochemical systems have been investigated. For example, divided electrochemical systems (Alvarez-Gallegos and Pletcher 1998, Gallegos et al. 2005, González-García et al. 2007, Lobyntseva et al. 2007, Qiang et al. 2002), fuel cell systems (Otsuka and Yamanaka 1990, Yamanaka et al. 2002, Yamanaka et al. 2003), and bioelectrochemical systems (Rozendal et al. 2009) have been studied to generate hydrogen peroxide. Furthermore, a solid polymer electrolyte (SPE) electrolyzer has been used to generate pure hydrogen peroxide (Murayama and Yamanaka

2011, Yamanaka and Murayama 2008). A membrane electrode assembly (MEA) is regarded as a core part of an SPE electrolyzer, and electrochemical reactions occur along a three-phase boundary (the intersection of Nafion-H electrolyte (liquid-like phase), electrode (solid), and oxygen (dissolved gas)) (Arihara et al. 2007, Takenaka et al. 1982, Yamanaka and Murayama 2008, Zhang et al. 2007).

Previous studies have reported generation of electrolyte-free hydrogen peroxide using the MEAs prepared in the SPE electrolyzer by the hot press method. However, those studies suffered from rather low current efficiency (~30%) (Murayama and Yamanaka 2011, Yamanaka and Murayama 2008). Few studies have employed coating electrode materials onto a mesh substrate to build MEAs to generate electrolyte-free hydrogen peroxide. We investigated high-yield hydrogen peroxide generation using electrode material-coated mesh substrates in an SPE electrolyzer. Current efficiency and power consumption while generating hydrogen peroxide in the MEA with a carbon fiber (CF)-coated stainless steel mesh substrate were examined and compared to the MEA prepared by the hot press method.

4.3.2. Current efficiency and H_2O_2 production in the SPE electrolyzer

Figure 4-13 shows the current efficiency of the SPE electrolyzer with the CFSS-MEA for hydrogen peroxide generation (20 min), compared to that with the CFNA-MEA (applied potential: -1.8 V, -1.4 V, -1.0 V, -0.5 V, -0.1 V). As shown in Fig. 4-13, the current efficiency of the SPE electrolyzer with the CFSS-MEA was much higher than that with the CFNA-MEA, despite the great variation in applied potential. For example, the current efficiency of the SPE electrolyzer with the CFSS-MEA increased to 55% at -0.1 V. In contrast, the current efficiency of the SPE electrolyzer with the CFNA-MEA was overall low at 2–7%. The occurrence of the best current efficiency at -0.1 V can be explained by competitive hydrogen formation below this negative potential. Note that the reduction potential of H_2 is -0.197 V.

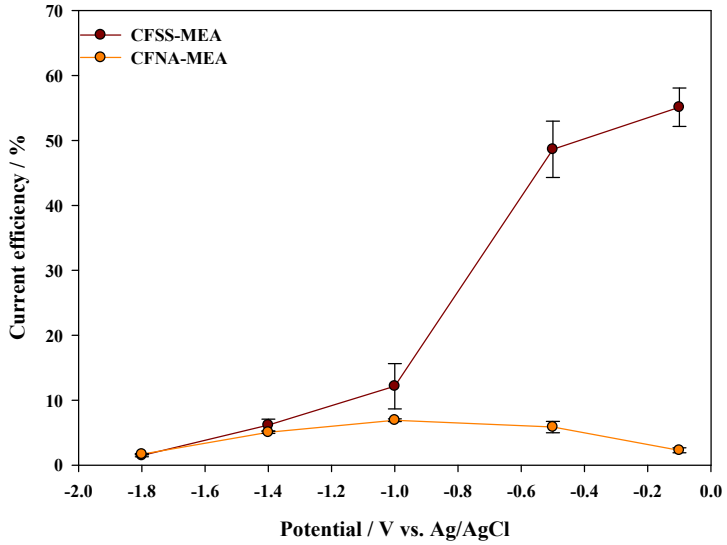

Figure 4-13. Current efficiency of hydrogen peroxide for the membrane electrode assembly with the carbon fiber coated stainless steel mesh (CFSS-MEA) and with the carbon fiber hot-pressed Nafion (CFNA-MEA) in the solid polymer electrolyte (SPE) electrolyzer (ultrapure water with O_2 sparging, electrolysis: 20 min).

Figure 4-14 shows hydrogen peroxide production of the SPE electrolyzer with the CFSS-MEA in comparison with that of the CFNA-MEA, as the electrolysis reaction was extended up to 3 hr at -0.1 V. These conditions represented the best current efficiency in the case of the CFSS-MEA. As shown in Fig. 4-14, hydrogen peroxide production for the CFSS-MEA was increased remarkably with time though that for the CFNA-MEA showed no increase in hydrogen peroxide production, which agreed with the results of Fig. 4-13. For example, hydrogen peroxide formation for the CFSS-MEA was 57 μg hr^{-1}·mg^{-1} CF, whereas it was only 0.2 μg hr^{-1}·mg^{-1} CF for the CFNA-MEA. Current efficiency and power consumption in the case of the CFSS-MEA were 52% and 0.3 Wh g^{-1}, respectively. These values improved substantially compared to the reported values (31% in an SPE electrolyzer (Murayama and Yamanaka 2011), and 0.9 Wh g^{-1} in a bioelectrochemical system (Rozendal et al. 2009).

The apparent geometric areas of CFSS and CFNA are 5.4 cm^2 and 12 cm^2, respectively. The ratio of the geometric areas of the CFSS to the CFNA is around 0.45, but current efficiency of CFSS is better than that of CFNA. Thus, the increased current efficiency to produce H_2O_2 is not due to the increased effective electrode area on CFSS. In addition, it is expected that exposing the CFSS-MEA to air as opposed to that immersed in the ultrapure water will contribute to improving current efficiency further, as observed in the previous publications [2, 11].

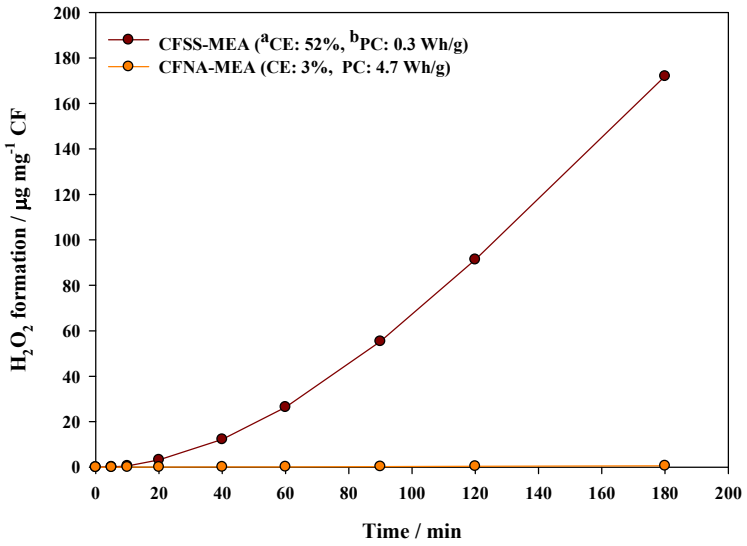

Figure 4-14. Hydrogen peroxide production for the membrane electrode assembly with the carbon fiber coated stainless steel mesh (CFSS-MEA) and with the carbon fiber hot-pressed Nafion (CFNA-MEA) in the solid polymer electrolyte (SPE) electrolyzer (-0.1 V vs. Ag/AgCl, ultrapure water with O_2 sparging)

a: current efficiency

b: power consumption

4.3.3. LSV and EIS in the SPE electrolyzer

Figure 4-15 shows LSV for the SPE electrolyzer with the CFSS-MEA and CFNA-MEA (scan rate, 160 mV s^{-1}; potential range, -1.8 V – -0.1 V). As shown in Fig. 4-15, cathodic current density for the CFSS-MEA was much higher than that for the CFNA-MEA at all of applied potential ranges. For example, the current density of the CFSS-MEA and CFNA-MEA was obtained at -0.04 mA mg^{-1} CF and -0.004 mA mg^{-1} CF at -0.1 V, respectively. One explanation for the enhanced current density of the CFSS-MEA in Fig. 4-15 was the significantly increased oxygen mass transfer through the well arranged voids resulting from a structural advantage of the CFSS-MEA (Fig. 3-4 (a)) at the three-phase boundary where electrochemical reactions occur in an SPE electrolyzer (Arihara et al. 2007, Yamanaka and Murayama 2008, Zhang et al. 2007).

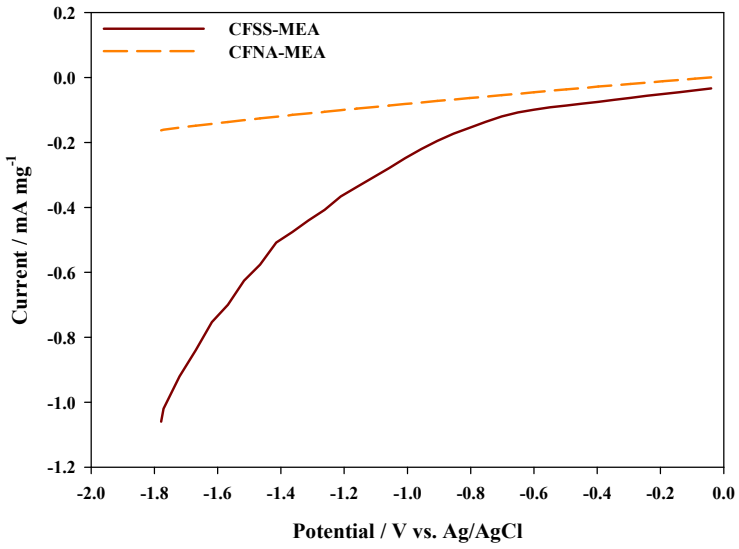

Figure 4-15. Linear sweep voltammograms for the membrane electrode assembly with the carbon fiber coated stainless steel mesh (CFSS-MEA) and with the carbon fiber hot-pressed Nafion (CFNA-MEA) in the solid polymer electrolyte (SPE) electrolyzer (O_2-saturated ultrapure water, 160 mV s^{-1})

Figure 4-16 shows the electrochemical impedance spectrum of the SPE electrolyzer with the CFSS-MEA, compared to that with the CFNA-MEA at -0.1 V (frequency, 5 Hz–200 kH). As shown in Fig. 4-16, the diameter of the low frequency arc for the CFSS-MEA was considerably smaller than that for the CFNA-MEA, indicating a small charge transfer resistance of the CFSS-MEA that contributed to good current efficiency and energy consumption. Note that no significant difference in the high frequency intercepts for the two MEAs was observed. The charge transfer resistance for the CFSS-MEA was as small as 20 ohm compared to that of the CFNA-MEA. This low charge transfer resistance for the CFSS-MEA is one reason for the high efficiency of hydrogen peroxide generation observed in Fig. 4-13.

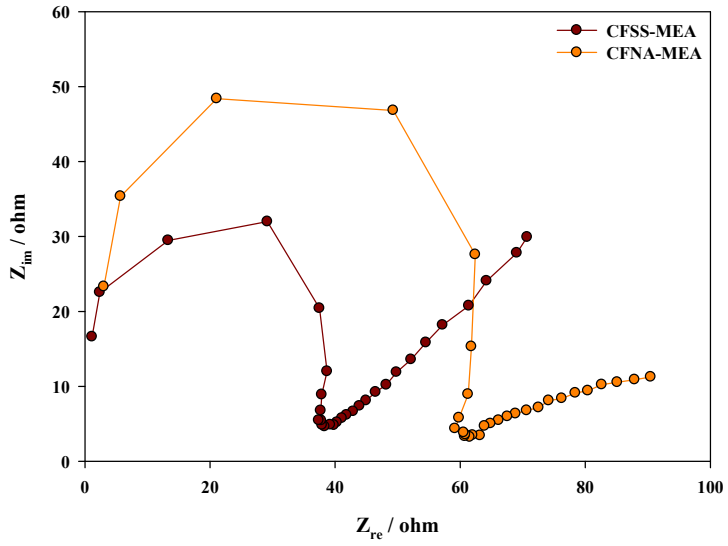

Figure 4-16. Electrochemical impedance spectroscopy for the membrane electrode assembly with the carbon fiber coated stainless steel mesh (CFSS-MEA) and with the carbon fiber hot-pressed Nafion (CFNA-MEA) in the solid polymer electrolyte (SPE) electrolyzer (at -0.1 V vs. Ag/AgCl, frequency: 5 Hz–200 kH, O_2-saturated ultrapure water)

4.3.4. Conclusions

We investigated high-yield hydrogen peroxide generation by the SPE electrolyzer with the CFSS-MEA. Current efficiency (52%) and power consumption (0.3 Wh g^{-1}) for this MEA were 1.5 times higher and 2 times lower than reported values, (at -0.1 V vs. Ag/AgCl). The better oxygen mass transfer and small charge transfer resistance arising from the well arranged voids resulting from the structural advantage of the CFSS-MEA explained these improvements.

4.4. Electrolyte-Free Hydrogen Peroxide Generation Using arbon Cloth Electrodes in a Solid Polymer Electrolyte Electrolyzer

4.4.1. Background

Hydrogen peroxide leaves no harmful chemicals after reaction and is an environmental friendly oxidant that has been used in many fields such as pulp bleaching, textiles, and advanced oxidation processes (Murayama and Yamanaka 2011, Qiang et al. 2002). Hydrogen peroxide is mainly produced by the anthraquinone process, but this process has several drawbacks such as formation of by-products and high operating cost. Transporting and handling concentrated hydrogen peroxide could be safety issues for the anthraquinone process as well (Gallegos et al. 2005, Lobyntseva et al. 2007). For these reasons, an on-site, energy efficient, and high purity hydrogen peroxide generation system is necessary.

An electrochemical system is considered one of the candidates for generating hydrogen peroxide through the oxygen reduction reaction, and several efforts to develop this type of system have been made. For example, hydrogen peroxide has been generated in divided electrochemical systems (Alvarez-Gallegos and Pletcher 1998, Gallegos et al. 2005, González-García et al. 2007, Lobyntseva et al. 2007, Qiang et al. 2002), fuel cell systems (Otsuka and Yamanaka 1990, Yamanaka et al. 2002, Yamanaka et al. 2003), and bioelectrochemical systems (Rozendal et al. 2009). However, the impurity of the hydrogen peroxide solution

should be considered due to anodic and cathodic reactions occurring in the presence of aqueous electrolyte. Thus, separate processes for producing pure hydrogen peroxide are required in those systems. Solid polymer electrolyte (SPE) electrolyzers have been suggested to overcome this problem (Murayama and Yamanaka 2011, Yamanaka and Murayama 2008).

Nafion that was sandwiched between a cathode and an anode has been employed as the electrolyte when designing SPE electrolyzers, and permits no use of aqueous supporting electrolyte (Cruz et al. 2011, Rasten et al. 2003). Thus, the impurity issue is excluded when ultrapure water for electrolysis is used to produce hydrogen peroxide. Hydrogen peroxide in ultrapure water is produced without any impurities in the SPE electrolyzer through the reduction of oxygen on a cathode ($O_2 + 2H^+ + 2e = H_2O_2$ at 0.68 V vs. NHE) while water is oxidized on an anode to form oxygen and proton that passes through Nafion ($O_2 + 4H^+ + 4e = 2H_2O$ at 1.23 V vs. NHE).

A carbon cathode for producing hydrogen peroxide is considered one of the best electrode materials due to its economic feasibility and environmental concerns (Alvarez-Gallegos and Pletcher 1998, Meinero and Zerbinati 2006, Sánchez-Sánchez and Bard 2009). Although carbon fiber electrodes prepared by a hot-press method have been employed for electrolyte-free hydrogen peroxide production in an SPE electrolyzer (Choi et al. 2013, Murayama and Yamanaka 2011, Yamanaka and Murayama 2008), few studies have been reported free-standing commercial

carbon cloth electrodes that are enable to be prepared in easy manner. We investigated electrolyte-free hydrogen peroxide production using carbon cloth in the SPE electrolyzer as three types of carbon cloth electrodes (carbon cloth, perforated carbon cloth, and stranded carbon cloth electrodes) were employed.

4.4.2. Current efficiency for carbon cloth electrodes in an SPE electrolyzer

Figure 4-17 (a) and (b) show hydrogen peroxide formation and current efficiency of all the three type of carbon cloth electrodes, respectively, as the potential was applied at -1.8 V for 20 min (electrodes: CC, 8PC, 16PC, 25PC, 1SC, 2SC, 3SC, 5SC, and 10SC). As shown in Fig. 4-17 (a) and (b), hydrogen peroxide formation and current efficiency of stranded carbon cloth electrodes among was superior among three types of electrode although hydrogen peroxide formation and current efficiency of perforated carbon cloth electrodes was slightly better than that of the CC. For example, the hydrogen peroxide formation of the stranded electrodes was observed at 0.34 – 0.62 μg/min/mg carbon cloth, whereas that of the other electrodes was obtained at < 0.03 μg/min/mg carbon cloth. In addition, the current efficiency of the stranded electrodes was 2–11%, whereas that of the perforated carbon cloth electrodes was < 2%. Note that that of carbon cloth was the lowest at 0.2%.

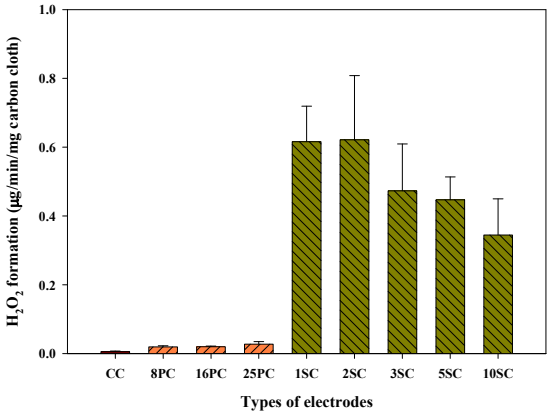

(a)

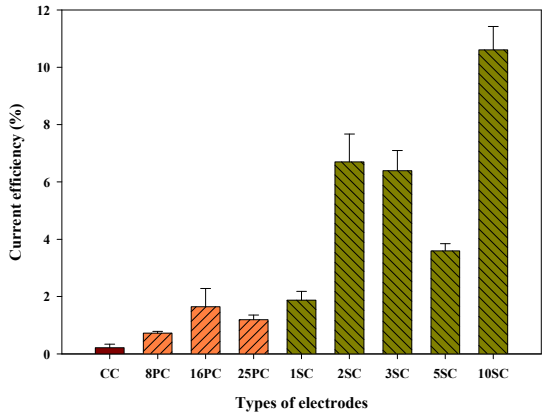

(b)

Figure 4-17. (a) Hydrogen peroxide formation and (b) current efficiency of carbon cloth, perforated carbon cloth, and stranded carbon cloth electrodes in an solid polymer electrolyte (SPE) electrolyzer (Electrodes: CC, 8PC, 16PC, 25PC, 1SC, 2SC, 3SC, 5SC, and 10SC, applied potential: -1.8 V (vs. Ag/AgCl), solution volume: 75 mL of ultrapure water, mixing: 600 rpm, electrolysis time: 20 min)

Since current efficiency at high negative potential is unflavored, current efficiency was investigated as applied potentials varied. Figure 4-18 shows the hydrogen peroxide production current efficiency for 10SC that showed the best performance in Fig. 4-17 (b) as potentials were applied from -1.8 V to -0.1 V in an SPE electrolyzer (electrolysis: 20 min). As shown in Fig. 4-18, current efficiency decreased substantially as the applied potential decreased from -0.1 V to -1.8 V. For example, current efficiency at -0.1 V was 42% with the power consumption of 0.4 Wh/g, whereas that at -1.8 V was about 10% with the power consumption of 27 Wh/g. It is noted that hydrogen peroxide production at high current efficiency was slower than that at low current efficiency (data not shown).

Although the current efficiency for 10SC at -0.1 V remained low in comparison with the recent our publication (current efficiency: 52%) (Choi et al. 2013), improved current efficiency of 10SC can be expected in the consideration of previous publications (Murayama et al. 2011, Yamanaka and Murayama 2008). The performance of 10SC can be improved by exposing 10SC to air as opposed to that immersed in the ultrapure water owing to rapid mass transfer of gaseous oxygen more than mass transfer of oxygen in water. Also, heat treatment of carbon cloth would increase current efficiency because specific functional groups facilitating H_2O_2 formation are well developed on the carbon electrode.

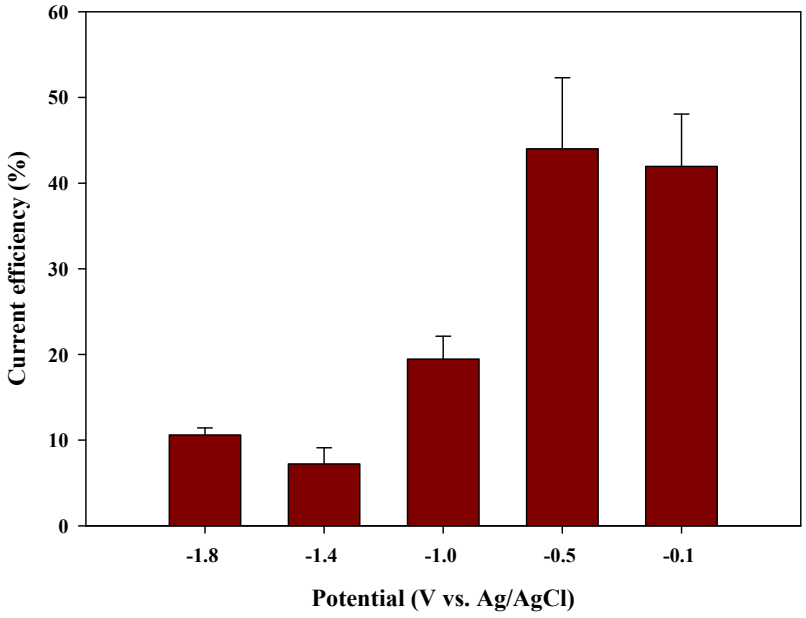

Figure 4-18. Hydrogen peroxide current efficiency for 10SC in a solid polymer electrolyte (SPE) electrolyzer at different applied potentials (applied potential: -1.8 V, -1.4 V, -1.0 V, -0.5 V, and -0.1 V vs. Ag/AgCl, solution volume: 75 mL of ultrapure water, mixing: 600 rpm, electrolysis time: 20 min)

4.4.3. CVs and Anson plots for CC, 25HC, and 10SC in an SPE electrolyzer

Figure 4-19 shows the CVs for selected carbon cloth electrodes with oxygen-saturated ultrapure water in the SPE electrolyzer (electrodes: CC, 25PC, and 10SC, scan rate: 160 $mV \cdot s^{-1}$, potential: -1.8 – 3.0 V). As shown in Fig. 4-19, current density for the 10SC was higher than that of the 25PC and CC, as potential varied from 0 V to -1.8 V. For example, the current densities for 10SC, 25PC, and CC were -0.46, -0.73, and 1.02 $mA \cdot mg^{-1}$ of carbon cloth at -1.8 V, respectively. This high current density for 10SC supports the result of Fig. 4-17 which shows higher current efficiency and formation of hydrogen peroxide for 10SC, as compared to that of the other carbon cloth electrodes.

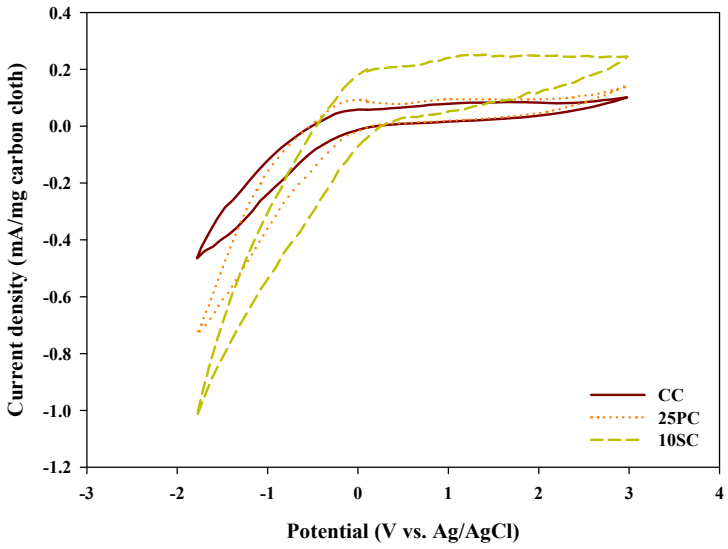

Figure 4-19. Cyclic voltammograms for CC, 25HC, and 10S in a solid polymer electrolyte (SPE) electrolyzer (solution volume: 75 mL of oxygen-saturated ultrapure water, scan rate: 160 $mV \cdot s^{-1}$)

Figure 4-20 shows the Anson plots for CC, 25PC and 10SC with oxygen-saturated ultrapure water in an SPE electrolyzer (potential step: 0 to -1.8 V). As shown in Fig. 4-20, the slopes of the Anson plots for 10SC appeared to be the lowest, and those for CC and 25PC were similar. The slope for 10SC was obtained at 2.8 × 10-4 $C \cdot s^{-1/2}$ whereas the slopes for CC and 25PC were 2.5 × 10-3 $C \cdot s^{-1/2}$ and 3.2 × 10-3 $C \cdot s^{-1/2}$, respectively. However, measured geometric active areas for those electrodes remained all similar based on the unit mass of employing carbon cloth (10SC: 6.2 × 10^{-4} $cm^2 \cdot mg^{-1}$, CC: 5.4 × 10^{-4} $cm^2 \cdot mg^{-1}$, 25PC: 7.1 × 10^{-4} $cm^2 \cdot mg^{-1}$).

10SC showing the highest current density even without the advantage of the geometric active area can be explained by increased oxygen mass transfer resulting from the distinguishing trait of the carbon cloth electrodes, as explained in our publication (Choi et al. 2013). 10SC might have good oxygen mass transfer to three-phase boundary which acts as reaction sites in the SPE electrolyzer (Arihara et al. 2007, Yamanaka and Murayama 2008, Zhang et al. 2007) due to many voids of 10SC in comparison with 25 PC and CC (Fig. 3-5), resulting in high current efficiency for 10 SC.

Commercially available carbon cloth itself will be a promising candidate for the electrode to produce hydrogen peroxide, but modifying the carbon cloth is necessary to achieve improved oxygen mass transfer, leading increased current efficiency.

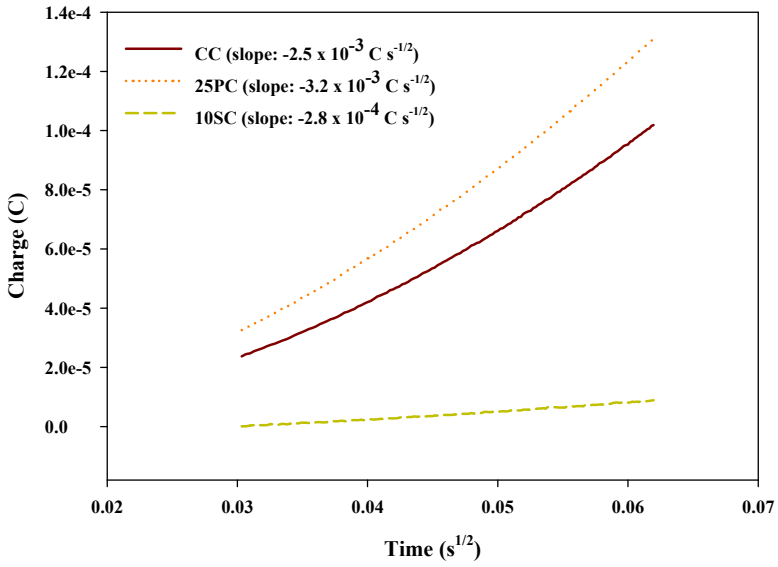

Figure 4-20. Anson plots for CC, 25HC, and 10S in a solid polymer electrolyte (SPE) electrolyzer (potential step: 0 to -1.8 V vs. Ag/AgCl, solution volume: 75 mL of oxygen-saturated ultrapure water)

4.4.4. Conclusions

In this study, electrolyte-free hydrogen peroxide production using carbon cloth electrodes in the SPE electrolyzer was investigated. Current efficiency and power consumption of hydrogen peroxide production for 10SC were 42% and 0.4 $Wh \cdot g^{-1}$ at - 0.1 V, respectively, whereas these for the other electrodes were substantially lower. This improved performance for 10SC can be attributed to the increased oxygen mass transfer. Modifying carbon cloth should be fully considered if carbon cloth is employed as the electrode for electrolyte-free hydrogen peroxide generation in the SPE electrolyzer.

5. Conclusions

This dissertation investigated the effect of SEs in EOP on a BDD electrode and development of electrodes for hydrogen peroxide production for efficient use of energy in an SPE electrolyzer. This has improved our knowledge in terms of potential impacts of supporting electrolytes on ozone production on BDD electrodes as well as the electrode development for hydrogen peroxide production.

- Effects of SEs on EOP on a BDD electrode were examined. When EOP in the presence of SE was compared to that in deionized water (DW), it was found that SE causes significant suppression of ozone production. However, the production of •OH and the overall oxidation current in CV did not decrease in the presence of SE, suggesting that hydroxyl radical formation is not inhibited by SE. On the contrary, the production of hydrogen peroxide via the recombination of •OH was suppressed by the SE. The suppression of EOP by SE is believed to be attributed to SE anions that hinder the recombination of •O on the electrode surface.
- Operating conditions for optimal yield EOP were investigated. Low electrical conductivity (0.001 $mS \cdot cm^{-1}$) led to effective EOP; high current efficiency (~14 %) of EOP was achieved on the BDD electrode under the conditions of 1A and 200 $mL \cdot min^{-1}$ 4℃ as compared to that on the PbO_2 electrode (4%). However, increasing electrical conductivity of solutions from 0.001 to 30

$mS \cdot cm^{-1}$ linearly reduced EOP on the BDD while EOP on the PbO_2 electrode was slightly decreased with the conductivity from 0.001 to 0.4 $mS \cdot cm^{-1}$, and then recovered at 30 $mS \cdot cm^{-1}$. At low electrical conductivity (0.001 – 0.4 $mS \cdot cm^{-1}$), BDD electrodes would allow high yield EOP, but PbO_2 electrodes would become effective at high electrical conductivity for EOP (> 30 $mS \cdot cm^{-1}$).

- High-yield hydrogen peroxide generation using a membrane electrode assembly (MEA) with a carbon fiber (CF)-coated mesh substrate was investigated in a solid polymer electrolyte electrolyzer. Current efficiency (52%) and power consumption (0.3 Wh g-1) for this MEA were 1.5 times higher and 2 times lower at -0.1 V vs. Ag/AgCl than those of reported values. These significant improvements were presumed to be attributed to enhanced oxygen mass transfer and reduced charge transfer resistance arising from the CF-coated mesh substrate in the MEA.
- Electrolyte-free hydrogen peroxide production using three types of carbon cloth electrodes (carbon cloth, perforated carbon cloth, and stranded carbon cloth electrodes) was investigated in the SPE electrolyzer. The stranded carbon cloth electrode achieved cathodic current efficiency of 42% and power consumption of 0.4 Wh/g, which were improved in comparison with the other types of electrodes. This can be attributed to increased oxygen mass transfer resulting from modifying carbon cloth electrodes, indicating that carbon cloth

for hydrogen peroxide production should be modified to achieve improved current efficiency in the SPE electrolyzer.

References

Alvarez-Gallegos, A. and Pletcher, D. (1998) The removal of low level organics via hydrogen peroxide formed in a reticulated vitreous carbon cathode cell, Part 1. The electrosynthesis of hydrogen peroxide in aqueous acidic solutions. Electrochimica Acta 44(5), 853-861.

Amadelli, R., Armelao, L., Velichenko, A., Nikolenko, N., Girenko, D., Kovalyov, S. and Danilov, F. (1999) Oxygen and ozone evolution at fluoride modified lead dioxide electrodes. Electrochimica Acta 45(4-5), 713-720.

Anson, F.C. (1966) Innovations in the Study of Adsorbed Reactants by Chronocoulometry. Analytical Chemistry 38(1), 54-57.

Arihara, K., Terashima, C. and Fujishima, A. (2006) Application of Freestanding Perforated Diamond Electrodes for Efficient Ozone-Water Production. Electrochemical and Solid-State Letters 9(8), D17-D20.

Arihara, K., Terashima, C. and Fujishima, A. (2007) Electrochemical production of high-concentration ozone-water using freestanding perforated diamond electrodes. Journal of The Electrochemical Society 154, E71.

Awad, M.I., Saleh, M.M. and Ohsaka, T. (2006) Ozone electrogeneration on Pt-loaded reticulated vitreous carbon using flooded and flow-through assembly. Journal of The Electrochemical Society 153(12), D207-D212.

Babak, A., Amadelli, R., De Battisti, A. and Fateev, V. (1994) Influence of anions on oxygen/ozone evolution on PbO_2/spe and PbO_2/Ti electrodes in neutral

pH media. Electrochimica Acta 39(11), 1597-1602.

Bader, H. and Hoigné, J. (1981) Determination of ozone in water by the indigo method. Water Research 15(4), 449-456.

Baga, A.N., Johnson, G.R.A., Nazhat, N.B. and Saadalla-Nazhat, R.A. (1988) A simple spectrophotometric determination of hydrogen peroxide at low concentrations in aqueous solution. Analytica Chimica Acta 204(0), 349-353.

Bard, A.J., Parsons, R. and Jordan, J. (1985) Standard potentials in aqueous solutions, CRC press.

Brillas, E. (2011) Synthetic diamond films: preparation, electrochemistry, characterization and applications, Wiley. com.

Buxton, G.V., Greenstock, C.L., Helman, W.P. and Ross, A.B. (1988) Critical review of rate constants for reactions of hydrated electrons, hydrogen atoms and hydroxyl radicals. Phys. Chem. Ref. Data 17, 513-886.

Cao, J., Zhao, H., Cao, F. and Zhang, J. (2007) The influence of F^- doping on the activity of PbO_2 film electrodes in oxygen evolution reaction. Electrochimica Acta 52(28), 7870-7876.

Cheng, S.A. and Chan, K.Y. (2004) Electrolytic generation of ozone on an antimony-doped tin dioxide coated electrode. Electrochemical and Solid-State Letters 7(3), D4-D6.

Cho, M., Chung, H., Choi, W. and Yoon, J. (2005) Different inactivation behaviors of MS-2 phage and Escherichia coli in TiO_2 photocatalytic disinfection.

Applied and Environmental Microbiology 71(1), 270-275.

Cho, M., Chung, H., Choi, W. and Yoon, J. (2004) Linear correlation between inactivation of E. coli and OH radical concentration in TiO_2 photocatalytic disinfection. Water Research 38(4), 1069-1077.

Choi, J., Hwang, S.H., Jang, J. and Yoon, J. (2013) High yield hydrogen peroxide production in a solid polymer electrolyte electrolyzer with a carbon fiber coated mesh substrate. Electrochemistry Communications 30(0), 95-98.

Comninellis, C. (1994a) Electrocatalysis in the electrochemical conversion/combustion of organic pollutants for waste water treatment. Electrochimica Acta 39(11), 1857-1862.

Comninellis, C. (1994b) Electrocatalysis in the electrochemical conversion/combustion of organic pollutants for waste water treatment. Electrochimica Acta 39(11-12), 1857-1862.

Cruz, J., Baglio, V., Siracusano, S., Ornelas, R., Ortiz-Frade, L., Arriaga, L., Antonucci, V. and Aricò, A. (2011) Nanosized IrO_2 electrocatalysts for oxygen evolution reaction in an SPE electrolyzer. Journal of Nanoparticle Research 13(4), 1639-1646.

Cui, Y., Wang, Y., Wang, B., Zhou, H., Chan, K.Y. and Li, X.Y. (2009) Electrochemical generation of ozone in a membrane electrode assembly cell with convective flow. Journal of The Electrochemical Society 156(4), E75-E80.

Da Silva, L.M., De Faria, L.A. and Boodts, J.F.C. (2003a) Electrochemical ozone production: influence of the supporting electrolyte on kinetics and current efficiency. Electrochimica Acta 48(6), 699-709.

Da Silva, L.M., Franco, D.V., Forti, J.C., Jardim, W.F. and Boodts, J.F.C. (2006) Characterisation of a laboratory electrochemical ozonation system and its application in advanced oxidation processes. Journal of Applied Electrochemistry 36(5), 523-530.

Da Silva, L.M., Franco, D.V., Sousa, L.G. and Gonçalves, I.C. (2010) Characterization of an electrochemical reactor for the ozone production in electrolyte-free water. Journal of Applied Electrochemistry 40(4), 855-864.

Da Silva, L.M. and Jardim, W.F. (2006) Trends and strategies of ozone application in environmental problems. Química Nova 29(2), 310-317.

Da Silva, L.M., Santana, M.H.P. and Boodts, J.F.C. (2003b) Electrochemistry and green chemical processes: electrochemical ozone production. Química Nova 26(6), 880-888.

El-Morsi, T.M., Budakowski, W.R., Abd-El-Aziz, A.S. and Friesen, K.J. (2000) Photocatalytic degradation of 1, 10-dichlorodecane in aqueous suspensions of TiO2: a reaction of adsorbed chlorinated alkane with surface hydroxyl radicals. Environmental Science & Technology 34(6), 1018-1022.

Foller, P. and Bombard, R. (1995) Processes for the production of mixtures of caustic soda and hydrogen peroxide via the reduction of oxygen. Journal of

Applied Electrochemistry 25(7), 613-627.

Foller, P.C. and Goodwin, M.L. (1984) The Electrochemical Ceneration Of High Concentration Ozone For Small-Scale Applications.

Foller, P.C. and Tobias, C.W. (1982) The anodic evolution of ozone. Journal of The Electrochemical Society 129, 506.

Foller, P.C. and Tobias, C.W. (1981) Effect of electrolyte anion adsorption on current efficiencies for the evolution of ozone. The Journal of Physical Chemistry 85(22), 3238-3244.

Gallegos, A.A., García, Y.V. and Zamudio, A. (2005) Solar hydrogen peroxide. Solar Energy Materials and Solar Cells 88(2), 157-167.

Goñi-Urtiaga, A., Presvytes, D. and Scott, K. (2012) Solid acids as electrolyte materials for proton exchange membrane (PEM) electrolysis: Review. International Journal of Hydrogen Energy 37(4), 3358-3372.

González-García, J., Banks, C.E., Šljukić, B. and Compton, R.G. (2007) Electrosynthesis of hydrogen peroxide via the reduction of oxygen assisted by power ultrasound. Ultrasonics Sonochemistry 14(4), 405-412.

Grigoriev, S., Porembsky, V. and Fateev, V. (2006) Pure hydrogen production by PEM electrolysis for hydrogen energy. International Journal of Hydrogen Energy 31(2), 171-175.

Grimm, J., Bessarabov, D., Simon, U. and Sanderson, R. (2000) Characterization of doped tin dioxide anodes prepared by a sol–gel technique and their

application in an SPE-reactor. Journal of Applied Electrochemistry 30(3), 293-302.

Grubb, W. (1959) Batteries with solid ion exchange electrolytes. Journal of The Electrochemical Society 106, 275.

Grubb, W. and Niedrach, L. (1960) Batteries with Solid Ion-Exchange Membrane Electrolytes. Journal of The Electrochemical Society 107, 131.

Jang, J., Bae, J., Choi, M. and Yoon, S.-H. (2005) Fabrication and characterization of polyaniline coated carbon nanofiber for supercapacitor. Carbon 43(13), 2730-2736.

Kapałka, A., Fóti, G. and Comninellis, C. (2008) Kinetic modelling of the electrochemical mineralization of organic pollutants for wastewater treatment. Journal of Applied Electrochemistry 38(1), 7-16.

Keenan, C.R. and Sedlak, D.L. (2008) Factors affecting the yield of oxidants from the reaction of nanoparticulate zero-valent iron and oxygen. Environmental Science & Technology 42(4), 1262-1267.

Kim, S. and Choi, W. (2002) Kinetics and mechanisms of photocatalytic degradation of $(CH_3)_nNH_{4-n}^+$($0 \leq n \leq 4$) in TiO_2 suspension: The role of OH radicals. Environmental Science & Technology 36(9), 2019-2025.

Kotz, E. and Stucki, S. (1987) Ozone and oxygen evolution on PbO_2 electrodes in acid solution. Journal of electroanalytical chemistry and interfacial

electrochemistry 228(1-2), 407-415.

Kraft, A., Stadelmann, M., Wünsche, M. and Blaschke, M. (2006) Electrochemical ozone production using diamond anodes and a solid polymer electrolyte. Electrochemistry Communications 8(5), 883-886.

Lee, C. and Yoon, J. (2004) Temperature dependence of hydroxyl radical formation in the *hv*/Fe^{3+}/H_2O_2 and Fe^{3+}/H_2O_2 systems. Chemosphere 56(10), 923-934.

Lee, J.S., Kwon, O.S., Park, S.J., Park, E.Y., You, S.A., Yoon, H. and Jang, J. (2011) Fabrication of Ultrafine Metal-Oxide-Decorated Carbon Nanofibers for DMMP Sensor Application. ACS Nano 5(10), 7992-8001.

Lobyntseva, E., Kallio, T., Alexeyeva, N., Tammeveski, K. and Kontturi, K. (2007) Electrochemical synthesis of hydrogen peroxide: Rotating disk electrode and fuel cell studies. Electrochimica Acta 52(25), 7262-7269.

Longsworth, L. (1960) The mutual diffusion of light and heavy water. The Journal of Physical Chemistry 64(12), 1914-1917.

Marselli, B., Garcia-Gomez, J., Michaud, P.A., Rodrigo, M.A. and Comninellis, C. (2003) Electrogeneration of Hydroxyl Radicals on Boron-Doped Diamond Electrodes. Journal of The Electrochemical Society 150(3), D79-D83.

Martínez-Huitle, C.A., De Battisti, A., Ferro, S., Reyna, S., Cerro-López, M.n. and Quiro, M.A. (2008) Removal of the pesticide methamidophos from aqueous solutions by electrooxidation using Pb/PbO_2, Ti/SnO_2, and Si/BDD

electrodes. Environmental Science & Technology 42(18), 6929-6935.

Masten, S.J., Galbraith, M.J. and Davies, S.H. (1996) Oxidation of 1, 3, 5-trichlorobenzene using advanced oxidation processes. Ozone: science & engineering 18(6), 535-547.

Meinero, S. and Zerbinati, O. (2006) Oxidative and energetic efficiency of different electrochemical oxidation processes for chloroanilines abatement in aqueous medium. Chemosphere 64(3), 386-392.

Michaud, P.A., Panizza, M., Ouattara, L., Diaco, T., Foti, G. and Comninellis, C. (2003) Electrochemical oxidation of water on synthetic boron-doped diamond thin film anodes. Journal of Applied Electrochemistry 33(2), 151-154.

Millet, P., Mbemba, N., Grigoriev, S., Fateev, V., Aukauloo, A. and Etiévant, C. (2011) Electrochemical performances of PEM water electrolysis cells and perspectives. International Journal of Hydrogen Energy 36(6), 4134-4142.

Mohd, Y. and Pletcher, D. (2006) The fabrication of lead dioxide layers on a titanium substrate. Electrochimica Acta 52(3), 786-793.

Murayama, T., Tazawa, S., Takenaka, S. and Yamanaka, I. (2011) Catalytic neutral hydrogen peroxide synthesis from O_2 and H_2 by PEMFC fuel. Catalysis Today 164(1), 163-168.

Murayama, T. and Yamanaka, I. (2011) Electrosynthesis of Neutral H_2O_2 Solution

from O_2 and Water at a Mixed Carbon Cathode Using an Exposed Solid-Polymer-Electrolyte Electrolysis Cell. The Journal of Physical Chemistry C 115(13), 5792-5799.

Nishiki, Y., Kitaori, N. and Nakamuro, K. (2011) Performances of small-sized generator of ozone-dissolved water using boron-doped diamond electrodes. Ozone: science & engineering 33(2), 114-120.

Onda, K., Ohba, T., Kusunoki, H., Takezawa, S., Sunakawa, D. and Araki, T. (2005) Improving characteristics of ozone water production with multilayer electrodes and operating conditions in a polymer electrolyte water electrolysis cell. Journal of The Electrochemical Society 152, D177.

Otsuka, K. and Yamanaka, I. (1990) One step synthesis of hydrogen peroxide through fuel cell reaction. Electrochimica Acta 35(2), 319-322.

Panizza, M. and Cerisola, G. (2007) Electrocatalytic materials for the electrochemical oxidation of synthetic dyes. Applied Catalysis B: Environmental 75(1), 95-101.

Panizza, M. and Cerisola, G. (2008) Electrochemical Degradation of Methyl Red Using BDD and PbO2 Anodes. Industrial & Engineering Chemistry Research 47(18), 6816-6820.

Qiang, Z., Chang, J.-H. and Huang, C.-P. (2002) Electrochemical generation of hydrogen peroxide from dissolved oxygen in acidic solutions. Water Research 36(1), 85-94.

Rajeshwar, K., Ibanez, J.G. and Swain, G.M. (1994) Electrochemistry and the environment. Journal of Applied Electrochemistry 24(11), 1077-1091.

Rasten, E., Hagen, G. and Tunold, R. (2003) Electrocatalysis in water electrolysis with solid polymer electrolyte. Electrochimica Acta 48(25-26), 3945-3952.

Rozendal, R.A., Leone, E., Keller, J. and Rabaey, K. (2009) Efficient hydrogen peroxide generation from organic matter in a bioelectrochemical system. Electrochemistry Communications 11(9), 1752-1755.

Rubin, M.B. (2001) The history of ozone. The Schönbein period, 1839–1868. Bull. Hist. Chem 26(1), 40-56.

Sánchez-Sánchez, C.M. and Bard, A.J. (2009) Hydrogen Peroxide Production in the Oxygen Reduction Reaction at Different Electrocatalysts as Quantified by Scanning Electrochemical Microscopy. Analytical Chemistry 81(19), 8094-8100.

Simond, O., Schaller, V. and Comninellis, C. (1997) Theoretical model for the anodic oxidation of organics on metal oxide electrodes. Electrochimica Acta 42(13), 2009-2012.

Sirés, I., Brillas, E., Cerisola, G. and Panizza, M. (2008) Comparative depollution of mecoprop aqueous solutions by electrochemical incineration using BDD and PbO_2 as high oxidation power anodes. Journal of Electroanalytical Chemistry 613(2), 151-159.

Siracusano, S., Baglio, V., Stassi, A., Ornelas, R., Antonucci, V. and Aricņ, A.

(2011) Investigation of IrO_2 electrocatalysts prepared by a sulfite-couplex route for the O_2 evolution reaction in solid polymer electrolyte water electrolyzers. International Journal of Hydrogen Energy.

Slade, S., Campbell, S., Ralph, T. and Walsh, F. (2002) Ionic conductivity of an extruded Nafion 1100 EW series of membranes. Journal of The Electrochemical Society 149(12), A1556-A1564.

Stucki, S., Baumann, H., Christen, H. and Kötz, R. (1987) Performance of a pressurized electrochemical ozone generator. Journal of Applied Electrochemistry 17(4), 773-778.

Stucki, S., Theis, G., Kötz, R., Devantay, H. and Christen, H. (1985) In situ production of ozone in water using a membrel electrolyzer. Journal of The Electrochemical Society 132, 367.

Sun, Y. and Pignatello, J.J. (1995) Evidence for a surface dual hole-radical mechanism in the titanium dioxide photocatalytic oxidation of 2, 4-D. Environmental Science & Technology 29(8), 2065-2072.

Takenaka, H., Torikai, E., Kawami, Y. and Wakabayashi, N. (1982) Solid polymer electrolyte water electrolysis. International Journal of Hydrogen Energy 7(5), 397-403.

Tanaka, K. (1978) Self-diffusion coefficients of water in pure water and in aqueous solutions of several electrolytes with 18O and 2H as tracers. J. Chem. Soc., Faraday Trans. 1 74, 1879-1881.

Tanaka, Y., Kikuchi, K., Saihara, Y. and Ogumi, Z. (2005) Investigation of current feeders for SPE cell. Electrochimica Acta 50(22), 4344-4349.

Tatapudi, P. and Fenton, J.M. (1994) Simultaneous Synthesis of Ozone and Hydrogen Peroxide in a Proton Exchange Membrane Electrochemical Reactor. Journal of The Electrochemical Society 141, 1174.

Tatapudi, P. and Fenton, J.M. (1993) Synthesis of ozone in a proton exchange membrane electrochemical reactor. Journal of The Electrochemical Society 140, 3527.

Tibaquirá, J.E., Hristovski, K.D., Westerhoff, P. and Posner, J.D. (2011) Recovery and quality of water produced by commercial fuel cells. International Journal of Hydrogen Energy 36(6), 4022-4028.

Ursúa, A., Gandía, L. and Sanchis, P. (2012) Hydrogen Production From Water Electrolysis: Current Status and Future Trends. Proceedings of the IEEE (99), 1-17.

Wabner, D. and Grambow, C. (1985) Reactive intermediates during oxindation of water lead dioxide and platinum electrodes. Journal of electroanalytical chemistry and interfacial electrochemistry 195(1), 95-108.

Wang, Y.H., Cheng, S., Chan, K.Y. and Li, X.Y. (2005) Electrolytic generation of ozone on antimony-and nickel-doped tin oxide electrode. Journal of The Electrochemical Society 152(11), D197-D200.

Wei, G., Xu, L., Huang, C. and Wang, Y. (2010) SPE water electrolysis with

SPEEK/PES blend membrane. International Journal of Hydrogen Energy 35(15), 7778-7783.

Weiss, E., Groenen-Serrano, K. and Savall, A. (2008) A comparison of electrochemical degradation of phenol on boron doped diamond and lead dioxide anodes. Journal of Applied Electrochemistry 38(3), 329-337.

Weiss, E., Groenen-Serrano, K. and Savall, A. (2006) Electrochemical degradation of sodium dodecylbenzene sulfonate on boron doped diamond and lead dioxide anodes. Journal of New Materials for Electrochemical Systems 9(3), 249.

Wu, G., More, K.L., Johnston, C.M. and Zelenay, P. (2011) High-Performance Electrocatalysts for Oxygen Reduction Derived from Polyaniline, Iron, and Cobalt. Science 332(6028), 443-447.

Wu, J.J. and Masten, S.J. (2002) Oxidation kinetics of phenolic and indolic compounds by ozone: applications to synthetic and real swine manure slurry. Water Research 36(6), 1513-1526.

Yamanaka, I., Hashimoto, T. and Otsuka, K. (2002) Direct Synthesis of Hydrogen Peroxide (>1 wt%) over the Cathode Prepared from Active Carbon and Vapor-Grown-Carbon-Fiber by a New H_2–O_2 Fuel Cell System. Chemistry Letters 31(8), 852-853.

Yamanaka, I. and Murayama, T. (2008) Neutral H_2O_2 Synthesis by Electrolysis of

Water and O_2. Angewandte Chemie International Edition 47(10), 1900-1902.

Yamanaka, I., Onizawa, T., Takenaka, S. and Otsuka, K. (2003) Direct and Continuous Production of Hydrogen Peroxide with 93% Selectivity Using a Fuel-Cell System. Angewandte Chemie International Edition 42(31), 3653-3655.

Zhang, Y., Wang, C., Wan, N., Liu, Z. and Mao, Z. (2007) Study on a novel manufacturing process of membrane electrode assemblies for solid polymer electrolyte water electrolysis. Electrochemistry Communications 9(4), 667-670.

Appendix

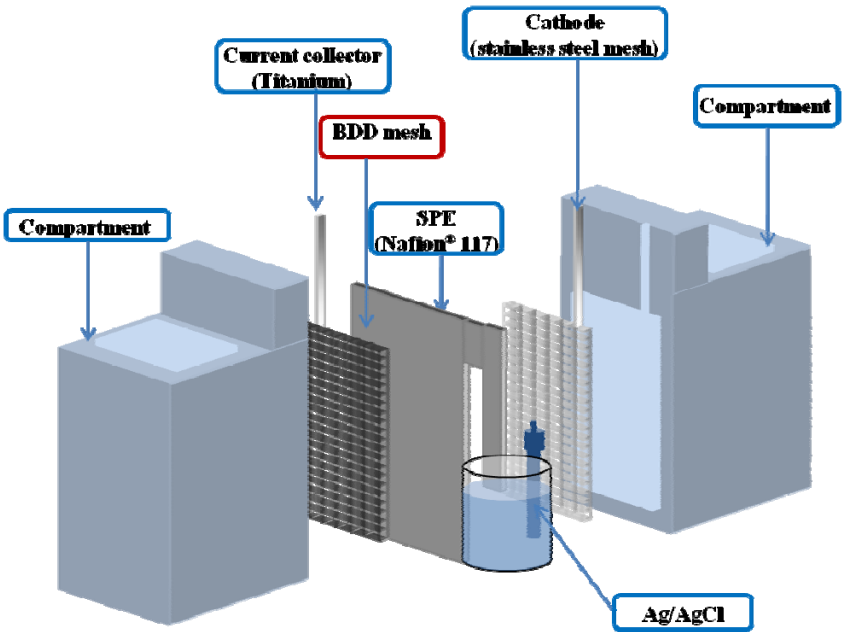

Figure S1. The configuration of the SPE electrolyzer

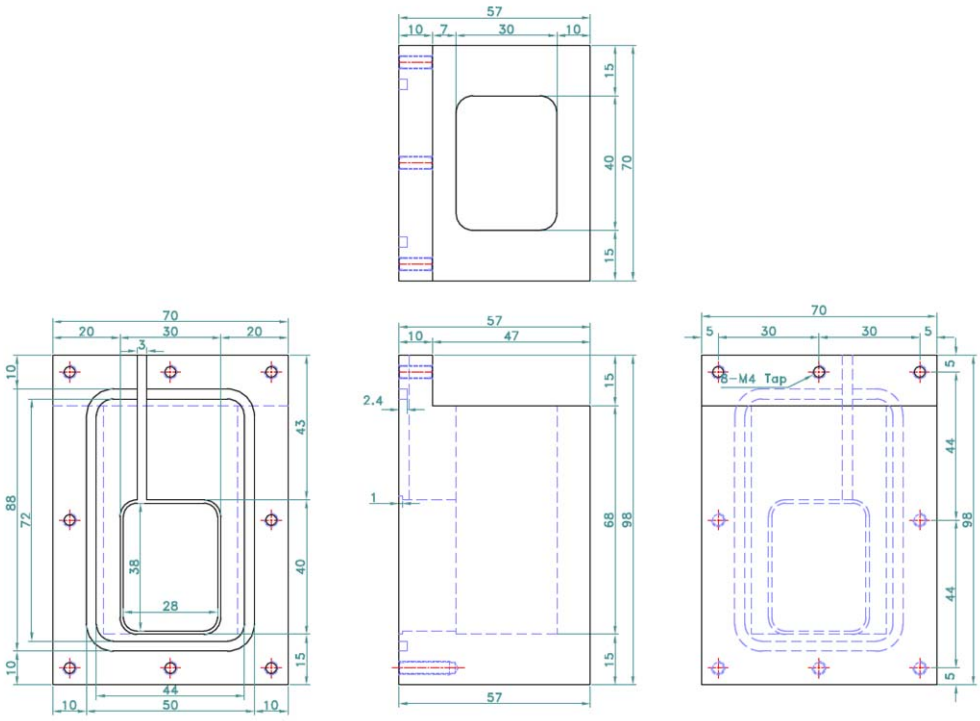

Figure S2. The blueprint of the SPE electrolyzer

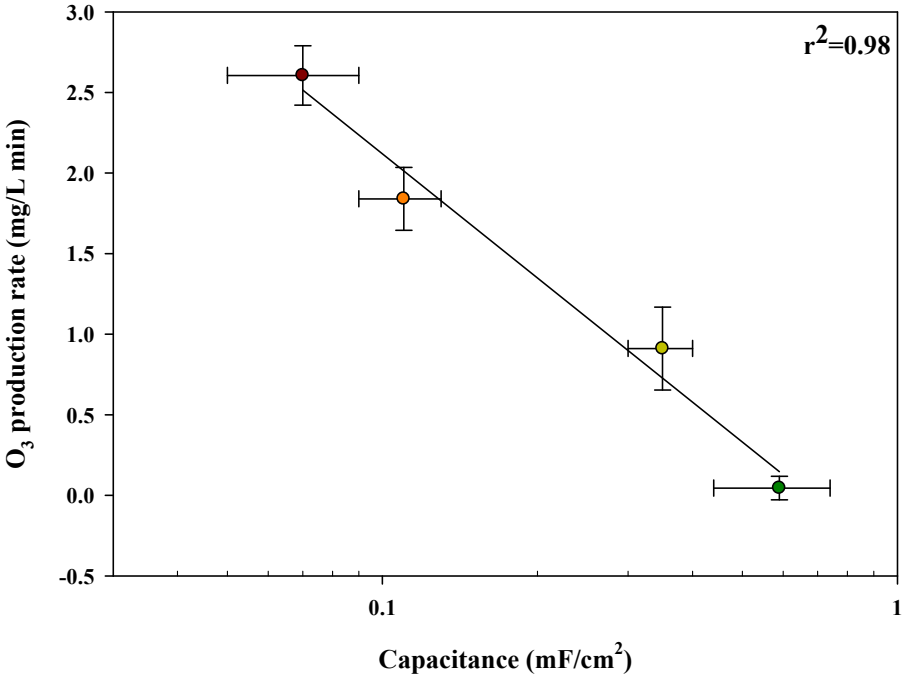

Figure S3. The relationship between ozone production rates and capacitance

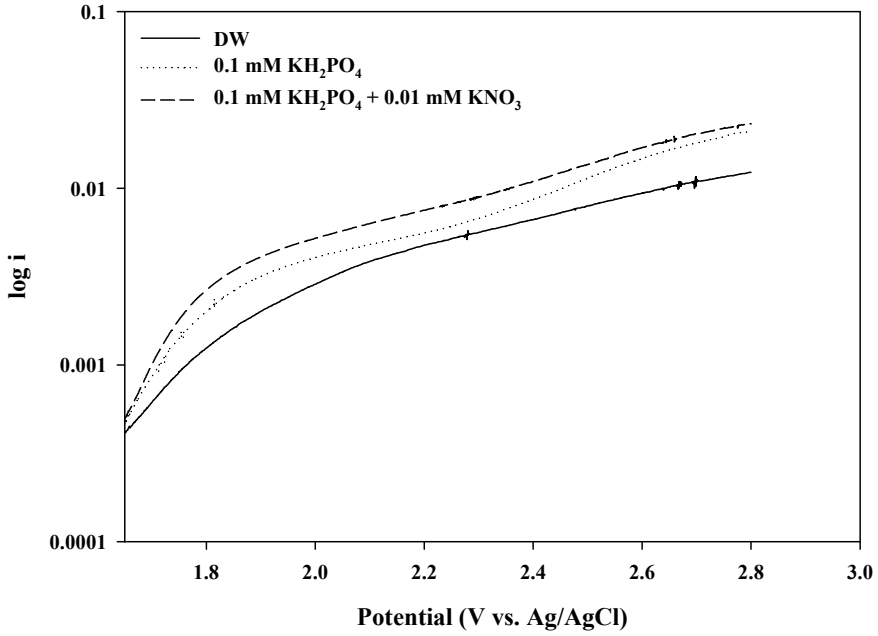

Figure S4. Tafel plots in 0.1 mM KH_2PO_4 and 0.1 mM KH_2PO_4 + 0.01 mM KNO_3 as compared that in DW.

Table S1. The potential measured during EOP

Electrolyte	100 mM	1 mM	0.01 mM	[a]0 mM
	Measured cell potential during EOP (V)			
KH_2PO_4	4.6	6.4	6.9	
KNO_3	4.4	7.5	7.3	
$HClO_4$	3.7	4.4	7.3	8.1
NaF	4.3	4.4	7.0	
HPF_6	4.0	4.4	7.8	

a: no electrolytes (deionized water)

국문 초록

전기화학적 오존생성은 기존의 오존생성 방법을 대체할 만한 효과적인 기술로 주목 받고 있다. 물의 산화로 발생되는 오존생성에서 보조전해질의 존재는 물의 전도도를 높이기 위해서 필수적이지만 다이아몬드 전극을 이용한 전기화학적 오존생성에서 보조전해질의 역할에 대한 이해는 부족하다. 또한 전기화학 반응을 효과적으로 이용하기 위해서는 산소의 환원으로 발생되는 과산화수소 생성용 전극 개발이 필요하다. 따라서 본 학위논문에서는 다음과 같은 연구를 수행하였다.

첫째, 다이아몬드 전극을 이용한 전기화학적 오존생성에서 보조전해질의 영향에 대해서 조사하였다. 보조전해질이 존재하지 않아도 물의 전기분해가 가능한 고체고분자전해질 전해조를 이용하였다. 주요 결과로는, 보조전해질이 존재하는 경우의 전기화학적 오존생성은 보조전해질이 존재하지 않는 경우에 비해 보조전해질의 종류에 상관없이 전기화학적 오존생성을 억제하였다. 그러나 보조전해질은 오존생성의 중간물질인 수산화라디칼 생성은 억제하지 않았고, 전체 전기화학 반응의 변화에도 영향을 미치지 않았다. 반면에 수산화라디칼의 결합에 의해서 생성되는 과산화수소는 보조전해질에 의해서 생성이 억제 되었다. 보조전해질에 의한 전기화학적 오존생성의 억제는 보조전해질의 음이온이

산소원자라디칼의 결합을 방해한 것으로 해석할 수 있다. 이러한 보조 전해질의 억제를 바탕으로 최적의 오존생성 조건에 대해서 제시하였다.

다음으로, 카본파이버가 코팅된 채 전극을 포함한 막전극 조립체를 이용하여 고효율 과산화수소 생성 전극 개발에 대해서 연구하였다. 카본파이버가 코팅된 채전극을 이용한 경우 얻어진 전류효율 (52%) 및 에너지 소모량 (0.3 Wh/g)은 기존 문헌에 보고된 것들에 비해서 각각 1.5배 높고 2배 이상 낮았다. 전극의 성능이 개선된 것은 채전극의 구조적 특성에 기인하는 빠른 산소물질 전달 및 낮은 전자전달 저항으로 설명할 수 있다. 이것을 바탕으로 하여 상업용 카본클로스 전극을 이용하여 과산화수소 생성에 적용하였다.

주요어: 수산화라디칼, 오존, 과산화수소, BDD 전극, 카본파이버, 고체고분자전해질 전해조

학번: 2009-31267

감사의 글

박사학위 기간 동안 저에게 많은 도움을 주신 윤제용 교수님께 깊은 감사의 말씀을 드립니다. 그리고 학위심사를 위해 귀중한 시간 내어 주신 이정학 교수님, 성영은 교수님, 강경석 박사님, 이창하 교수님에게 감사의 말씀 드립니다. 또한, 박사학위를 받기까지 저에게 힘이 되어준 여러 사람들에게 감사의 말을 드리고 싶습니다. 우선, 학위 기간 동안 저를 뒷바라지 해준 아내에게 감사의 말을 하고 싶습니다. 미래에 저의 학위논문을 한번이라도 읽어볼 기회가 있을지 모르지만 시원이, 현재 엄마 뱃속에 있는 둘째 재원이에게 너희들이 있어서 항상 행복하단 말을 하고 싶습니다. 현재 저를 있게 해주신 부모님, 저의 아내를 있게 해주신 장인어른, 장모님, 그리고 큰누나, 큰매형, 작은누나, 작은매형, 그리고 하나뿐인 조카 소정이에게 감사의 말씀 드립니다. 그리고 실험실 생활을 하면서 가족보다도 더 오랜 시간을 보내면서 정든 현재 실험실 식구 모두에게 (강전일, 김태영, 백영빈, 김정찬, 김춘수, Luu, 김영민, 김성환, 유지현, 이재한, Wanacha, 윤홍식, 서동우, 조규식, 김지예, 김선이, 임민혁) 감사의 말을 전하고 싶습니다.

2014년 1월 연구실에서

최 주 솔 드림